

**CHARACTERIZATION OF SCHWANN CELLS STIMULATED BY DC
ELECTRIC FIELDS**

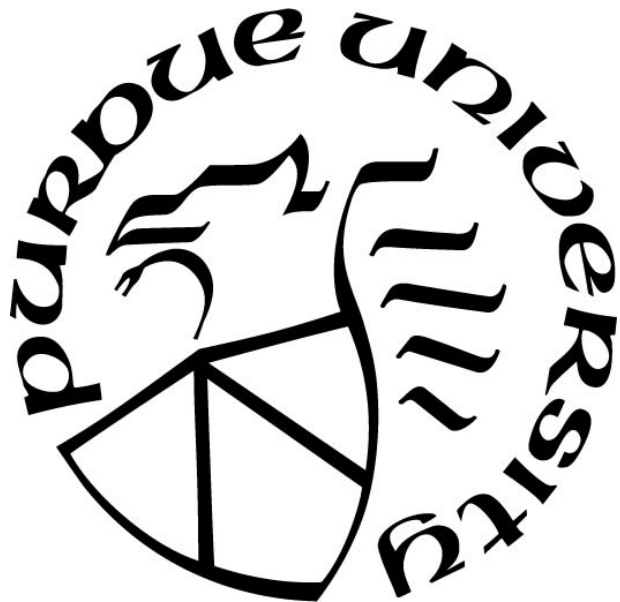
by
Spencer J. Bunn

A Thesis

Submitted to the Faculty of Purdue University

In Partial Fulfillment of the Requirements for the degree of

Master of Science in Biomedical Engineering



Weldon School of Biomedical Engineering

West Lafayette, Indiana

August 2019

**THE PURDUE UNIVERSITY GRADUATE SCHOOL
STATEMENT OF COMMITTEE APPROVAL**

Dr. Jianming Li, Co-Chair

Department of Basic Medical Sciences

Dr. Chi Hwan Lee, Co-Chair

Weldon School of Biomedical Engineering

Dr. Adrian Buganza

School of Mechanical Engineering

Approved by:

Dr. George R. Wodicka

Head of the Graduate Program

To my family – Mackenzie, Grayson, and my parents, Jared and Sharon. I cannot fully describe what your love and support mean to me.

ACKNOWLEDGMENTS

I would like to recognize the help of all who contributed to this work, as well as those who've sacrificed time to teach me. Dr. Adrian Buganza and Dr. Chi Hwan Lee, I sincerely thank each of you for your willingness to offer advice and listen throughout my research. I am extremely grateful for the guidance, support, and example of Dr. Jianming Li. I truly believe this learning experience you've helped shape will be invaluable to me.

To each of the current and previous members of the Center for Paralysis Research – Debra Bohnert, Kavya Cherukuri, John Cirillo, Jennifer Danaher, Michael Schweinsberg, Shruthi Suresh, and Michael Walls – thank you for helping make this research possible. I'd especially like to thank Bhavani Gopalakrishnan, Alexander Lai, Mary Lang, and Megan Sanger for their willing contributions to this research.

Lastly, I'd like to recognize my wife, Mackenzie, for her unwavering support.

TABLE OF CONTENTS

LIST OF TABLES	7
LIST OF FIGURES	8
ABBREVIATIONS	10
ABSTRACT.....	11
1. INTRODUCTION	13
1.1 The Peripheral Nervous System.....	13
1.1.1 Function & Classification	13
1.1.2 Structure.....	13
1.2 Peripheral Nerve Injuries	16
1.2.1 PNI Classification & Treatment	16
1.2.2 Pathophysiology of PNI.....	22
1.3 Electric Fields	25
1.3.1 Endogenous Electric Fields	25
1.3.2 Promoting Regeneration with Applied Electric Fields.....	25
1.3.3 Characterizing Electric Field-Stimulated Schwann Cells to Promote Peripheral Nerve Regeneration	29
2. APPLICATION OF ELECTRIC FIELDS TO SCHWANN CELL CULTURES	31
2.1 Introduction.....	31
2.2 Materials and Methods.....	31
2.2.1 Cell Culture.....	31
2.2.2 Electric Field Setup.....	33
2.2.3 Migration Tracking.....	35
2.2.4 Proliferation Rate & Angle of Cell Division	35
2.2.5 Alignment & Morphology	36
2.2.6 Immunofluorescence.....	37
2.2.7 Statistical Analysis.....	38
2.3 Results.....	38
2.3.1 Migration	38
2.3.1.1 Constant EFs.....	39

2.3.1.2	50% Duty Cycle EFs	39
2.3.1.3	Oscillating EFs	40
2.3.2	Proliferation Rate.....	42
2.3.3	Angle of Cell Division.....	42
2.3.4	Alignment	44
2.3.4.1	Con EFs	44
2.3.4.2	50% d.c. EFs.....	44
2.3.4.3	Osc EFs.....	44
2.3.5	Morphology	46
2.3.6	Primary Schwann Cell Comparison.....	46
2.3.7	Integrin β 1 Distribution	48
2.4	Discussion.....	49
2.5	Variable Cell Density.....	54
3.	SCHWANN CELL RESPONSE TO ELECTRIC FIELDS IN FIBRIN MATRICES.....	56
3.1	Introduction.....	56
3.2	Materials and Methods.....	58
3.2.1	PDMS Channel Slides	58
3.2.2	Cell Culture.....	59
3.2.3	Migration Tracking & Alignment.....	60
3.2.4	Statistical Analysis.....	60
3.3	Results.....	60
3.3.1	Migration	61
3.3.2	Alignment	62
3.4	Discussion.....	63
4.	CONCLUSIONS AND FUTURE DIRECTIONS	66
4.1	Conclusions.....	66
4.2	Future Directions	67
	APPENDIX.....	69
	REFERENCES	70
	PUBLICATIONS.....	77

LIST OF TABLES

Table 1 Schwann cell alignment data in 2D	45
Table 2 Schwann cell migration data in 3D fibrin matrices	62

LIST OF FIGURES

Figure 1.1 The central and peripheral nervous systems.....	14
Figure 1.2 Neuron structure	15
Figure 1.3 Glia of the peripheral nervous system	15
Figure 1.4 Peripheral nerve structure.....	16
Figure 1.5 Classifications of nerve injury.....	19
Figure 1.6 Epineurial neuroorrhaphy.....	20
Figure 1.7 Schematic of nerve autograft.....	20
Figure 1.8 Axogen Avance nerve graft.....	21
Figure 1.9 Nerve guidance conduits	21
Figure 1.10 Schematic of Wallerian degeneration.....	23
Figure 1.11 Schwann cells guiding an extending neural growth cone	24
Figure 1.12 Nerve regeneration with the Oscillating Field Stimulator.....	28
Figure 2.1 Electric field setup, calculation, and model.....	34
Figure 2.2 DC electric field stimulation regimes.....	34
Figure 2.3 Schwann cell migration tracking.....	35
Figure 2.4 Angle of cell division schematic	36
Figure 2.5 Cell alignment schematic	37
Figure 2.6 Migration in constant electric fields.....	39
Figure 2.7 Migration in 50% duty cycle electric fields	40
Figure 2.8 Migration in oscillating electric fields.....	41
Figure 2.9 Schwann cell proliferation in electric fields.....	42
Figure 2.10 Angle of cell division	43
Figure 2.11 Schwann cell alignment in electric fields.....	45
Figure 2.12 Schwann cell elongation.....	46
Figure 2.13 S100 protein expression in primary Schwann cells.....	47
Figure 2.14 Migration and alignment of primary Schwann cells	47
Figure 2.15 Integrin β 1 expression in Schwann cells	48
Figure 2.16 Schwann cell migration and alignment on poly-L-lysine.....	53
Figure 2.17 The effect of stimulation regime on Schwann cell alignment.....	53

Figure 2.18 The effect of cell density on Schwann cell alignment.....	55
Figure 3.1 Fibrin is upregulated after nerve injury	57
Figure 3.2 Custom PDMS channel slide.....	58
Figure 3.3 Schwann cell migration in fibrin matrices.....	61
Figure 3.4 Electric field induced Schwann cell alignment in fibrin.	62
Figure 4.1 Fibrinogen/fibrin structure.....	69

ABBREVIATIONS

50% Duty Cycle (50% d.c.)

Constant (Con)

Direct Current (DC)

Extracellular Matrix (ECM)

Electric Field (EF)

Integrin $\beta 1$ (IB1)

Oscillating (Osc)

Oscillating Field Stimulator (OFS)

Peripheral Nerve Injury (PNI)

Peripheral Nervous System (PNS)

Polydimethylsiloxane (PDMS)

Schwann Cell (SC)

Three-Dimensional Cell Culture (3DCC)

ABSTRACT

Author: Bunn, Spencer, J. MSBME
Institution: Purdue University
Degree Received: August 2019
Title: Characterization of DC Electric Field-Stimulated Schwann Cells
Committee Chair: Jianming Li, Chi Hwan Lee

Schwann cells (SCs) are PNS glia with numerous neuron-supporting functions, including myelination of axons. Although lesser discussed, SCs also fulfill many important roles after peripheral nerve injury (PNI) contributing significantly to the PNS regeneration process. Clusters of congregated SCs (Bands of Bungner) precede axon regeneration and facilitate the growth of extending axons to their distal targets which is particularly important in the lesion area of severed nerves. While this phenomenon occurs naturally, recovery from PNI can still be inadequate, especially in nerve transection or large gap injuries. Current treatments for nerve transection injuries are limited to coaptation of the nerve via sutures or nerve grafts. However, poor functional outcomes or donor site morbidity remain unaddressed problems. At the cellular level, axon pathfinding and extension relies heavily on the interaction between SCs and axonal growth cones. Depletion or removal of SCs at the lesion has been implicated to poor functional outcomes. With their pivotal role throughout nerve regeneration, we theorize axon regeneration can be improved by augmenting the SC population at the site of injury by encouraging migration to the lesion and via expression of morphological phenotypes that imitate the Bands of Bungner.

DC electric fields (EFs) have been well studied in the past as a method to modulate cell orientation and migration and within the context of the nervous system, have been used to promote regeneration in lesioned spinal cords. However, very little work has investigated the effects of electrical stimulation on glia, such as SCs. Existing literature is lacking with regards to various aspects of SC responses, including direction of alignment. We hypothesize electrical stimulation can modulate SC behavior to reinforce/replicate behaviors observed within Bands of Bungner, which may be developed into a treatment for victims suffering peripheral nerve injury.

We begin the current study with a thorough investigation into electric field modulated SC behavior. Using conventional 2D cell culture we demonstrate SC sensitivity to EFs by analyzing

alignment, morphology and migration data. We employed EFs within the physiologic range. Waveforms used were constant DC as well as a 50% duty cycle DC and an oscillating DC. The latter two may prove more appropriate *in vivo* due to reduced accumulation of cytotoxic byproducts generated at the electrode interfaces.

Our results highlight the sensitivity of SCs to DC electric fields of varying waveforms. SCs showed a strong propensity to align perpendicular to the field and display some cathodal migration in 2D cultures. Additional studies with variable cell density revealed cell-cell interaction further enhanced the alignment response. To more closely replicate the nerve microenvironment, a 3D cell culture model of PNI was created. Embedded in matrices, we found SCs displayed weaker migratory and alignment responses compared to 2D results. The direction of galvanotaxis was reversed, with SCs migrating toward the anode. Both alignment and migratory responses have potential applications for PNI. The galvanotactic behavior of SCs could be used to boost the SC population, increasing the number of Bands of Bungner. Cell alignment would be particularly advantageous at the lesion where axon regeneration is most difficult without the physical guidance of endoneurial tubes.

This study characterizes SC behavior in applied EFs using conventional 2D and 3D cell culture techniques. We found SCs are sensitive to electric stimulation, supporting the idea that applied EFs could be used to indirectly promote regeneration in damaged peripheral nerve by modulating SC response after injury. Potential applications include generating an EF across damaged nerves to align SCs, especially in the lesioned area, using EFs to induce SC migration to the lesion to increase the number of cells guiding severed axons, and pre-aligning SCs in synthetic nerve grafts.

1. INTRODUCTION

1.1 The Peripheral Nervous System

1.1.1 Function & Classification

The nervous system is a complex cellular network which utilizes electrical signals to rapidly transmit information across the body. The nervous system can be divided into two categories – the central nervous system (CNS) and peripheral nervous system (PNS) (Figure 1.1). The CNS consists of the brain and spinal cord and is the center of thoughts and cognition. The PNS is made up of all remaining nerves and is the wiring facilitating communication between the CNS and motor/sensory targets throughout the body.

Nerves of the PNS are categorized based on their function. Neuron bundles which elicit voluntary motor responses of muscle are called efferent or motor nerves. Efferent nerves relay electrical signals unidirectionally, descending from the CNS to muscle end plates. Afferent or sensory nerves transfer signals in the opposite direction – from sensory organs in the periphery to the CNS. A third classification within the PNS is autonomic nerve. Autonomic nerves are similar to motor nerves in that signals originate from the CNS and descend to the periphery; however, the distinction is made because autonomic nerves affect smooth muscle which is not controlled voluntarily. The sympathetic and parasympathetic nervous systems are comprised of autonomic nerves. Targets of autonomic nerves include smooth muscle in blood vessels, the gastrointestinal tract and various glands.

1.1.2 Structure

Though delicate and highly organized, peripheral nerve parenchyma is composed of only three cell types, specifically neurons, Schwann cells and satellite cells. Neurons are elongated electrically excitable cells which are directly responsible for signal transmission in the form of action potentials. Dendrites are short branched extensions of neurons responsible for receiving signals. From the dendrites, an action potential is relayed to the cell body or soma of the neuron, which contains the nucleus and other essential organelles. Long projection(s) responsible for transmitting electrical signals are called axons, these extensions can measure over 1 meter. The

generalized neuron anatomy is illustrated in Figure 1.2, though a variety of specialized neuron types exist.

All non-neural cells of the nervous system are collectively known as glia, a word meaning “glue” in Greek. The term fittingly describes the collective neuron supporting functions of glial cells. While there are various types in the CNS, the PNS has only two glia – Schwann cells and satellite cells (Figure 1.3). Schwann cells (SCs) are the most abundant cell in the PNS and have numerous roles including ensheathing myelinated axons, supporting neuron metabolism, and clearance of debris. Because of their size, a myriad of SCs is needed to properly myelinate a single axon. Remak SCs are a specialized subtype that support the function of multiple unmyelinated neurons. Satellite cells are PNS glia which associate exclusively with the neural cell body, providing protection and nutrition to the soma.

Peripheral nerves can contain thousands of individual axons arranged in a highly organized structure. Axons, whether myelinated or unmyelinated, are surrounded by a layer of connective tissue known as the endoneurium. Fascicles are bundles of endoneurial tubes surrounded by a second layer of connective tissue called the perineurium. All fascicles within a nerve are ensheathed by the outermost layer of connective tissue, the epineurium (Figure 1.4).

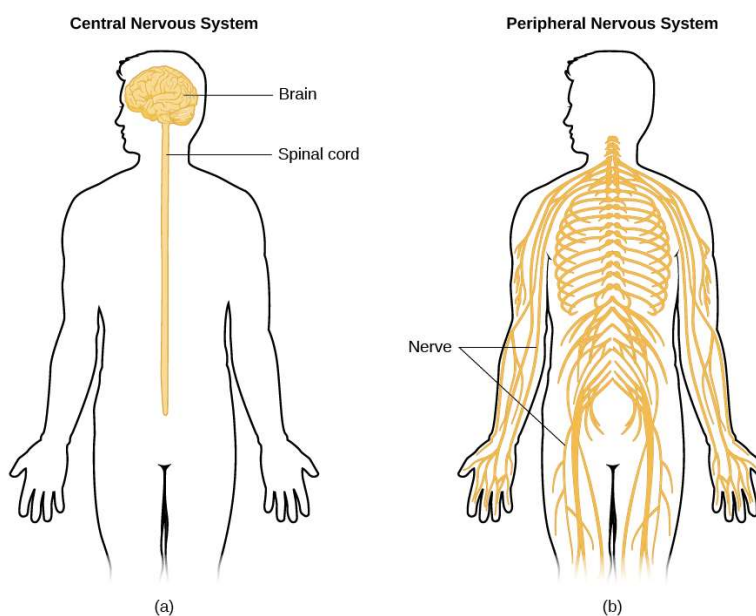


Figure 1.1 The central and peripheral nervous systems

The CNS is comprised of the brain and spinal cord, all other nerves are part of the PNS. Figure by OpenStax College is licensed under CC BY 4.0.

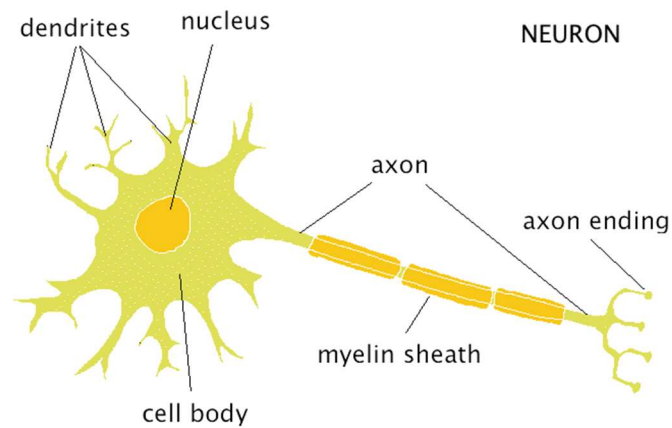


Figure 1.2 Neuron structure

Neurons contain many projections – dendrites which receive signals from other neurons or sensory organs and long axons which transmit the signal. © Dr. C. George Boeree.

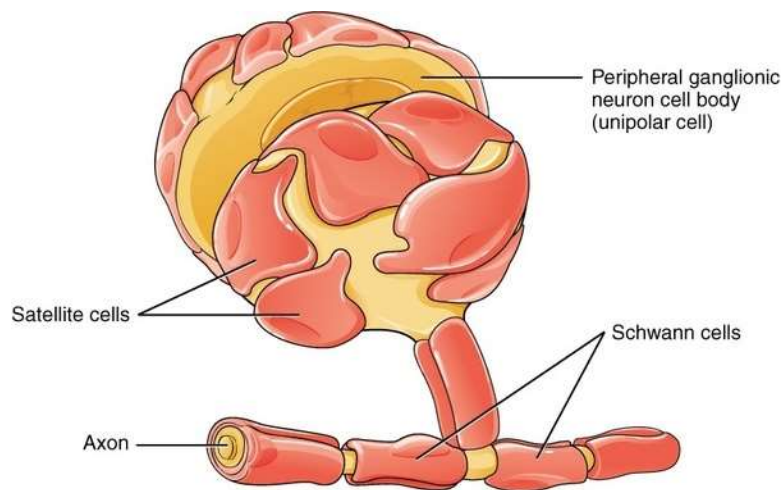


Figure 1.3 Glia of the peripheral nervous system

In healthy nerve, Schwann cells primary function is to insulate axons with a myelin sheath. Satellite cells offer protection and provide nutrients to the neural cell body. Figure by OpenStax College is licensed under CC BY 4.0.

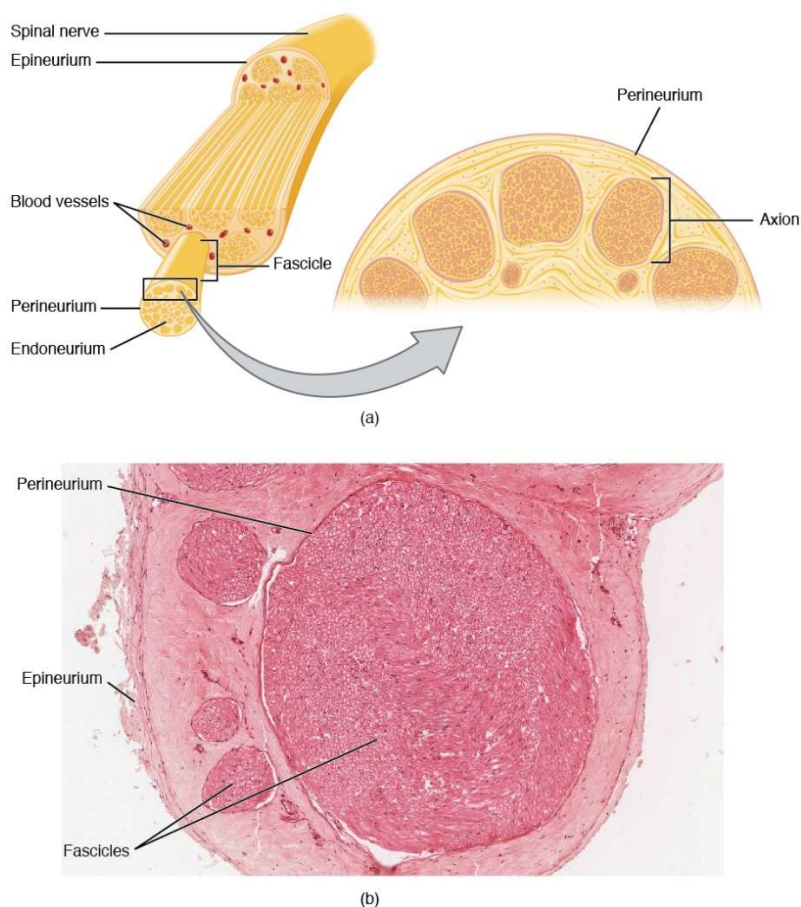


Figure 1.4 Peripheral nerve structure

Individual axons are surrounded by endoneurium. Bundles of axons are grouped in fascicles and surrounded by perineurium. The epineurium forms the outermost layer of connective tissue.

Figure by OpenStax College is licensed under CC BY 4.0.

1.2 Peripheral Nerve Injuries

1.2.1 PNI Classification & Treatment

By definition peripheral nerve injury (PNI) occurs when delicate tissue of peripheral nerve is damaged, preventing proper function. PNIs requiring treatment are often the result of physical trauma such as motor vehicle accidents. As of 2009, an estimated 550,000 Americans undergo surgical treatment for such injuries each year [1]. While peripheral neurons are capable of regenerating, recovery from PNIs depends largely on the location and extent of damage of the injury and consequently the prognosis varies enormously. Moderate injury often leads to short-term numbness and an eventual full recovery, while severe injuries can cause local paralysis with permanent loss of sensation and/or motor control.

There are two commonly accepted and closely related PNI classification systems (Figure 1.5). The first, developed by Herbert Seddon, consists of three levels of nerve injury [2]. The mildest form of injury, neuropraxia, causes a temporary signal conduction block but does not lead to degradation of any portion of the neurons. Neuropraxia may be caused by damage to SCs leading to demyelination of axons or prolonged compression causing nerve ischemia. Axontmesis is classified as injury causing damage to axons while leaving the surrounding connective tissue intact. Axontmesis leads to degradation of axons segments distal to the site of injury. The process of axon breakdown and clearance of debris in the distal nerve is called anterograde degeneration or Wallerian degeneration, named after its discoverer Augustus Waller. In the Seddon classification, neurotmesis is the most severe form of nerve injury and is defined as the complete disruption of axons and connective tissue or severance of the nerve fiber.

The PNI classification system developed by Sydney Sunderland is analogous to Seddon's, however it is more complex with five distinct levels (degrees) of nerve injury [3]. First degree nerve injury shares nearly the same description as neuropraxia, with no loss of axon continuity. Degrees two through five all include severance to the axon but differ in the extent of damage inflicted connective tissue microarchitecture. Second degree nerve injury causes axon damage but the endoneurium remains intact. Third degree injury is damage to axons as well as the endoneurium. Fourth degree nerve injury is characterized by damage to axons, endoneurium and perineurium while the epineurium is unbroken. Fifth degree nerve damage is defined by a disruption of the epineurium or complete nerve severance (similar to Sunderland's neurotmesis).

Selection of appropriate treatment for PNI is largely dependent on the severity of the injury. Neuropraxia or first-degree nerve injury causes only transient symptoms and a full recovery is expected sans medical intervention. Generally, no medical action is taken for axontmesis or second through fourth degree nerve injuries, as surgery would exacerbate the damage. Loss of motor function or sensation caused by fifth degree nerve injury or neurotmesis is irreversible unless treated. Recovery is dependent on the location of injury (proximal or distal) and extent of damage to the nerve tissue [4], [5]. Intuitively, injuries which are more distal and injure less nerve stroma have a better prognosis and satisfactory recovery of sensation and motor control are more likely.

Following neurotmesis or 5th degree nerve injury, medical intervention is required to reconnect severed nerves and make possible any sort of recovery. Multiple approaches exist for

nerve severance and, similar to prognosis, the treatment selection depends upon the physical state of the nerve damage. When the resulting gap in the nerve fiber is small, generally less than 4-5 mm, neurorrhaphy – re-approximating the transected nerve by suturing the epineurium or perineurium (Figure 1.6), is a well-established treatment method and is widely considered the gold standard approach by medical professionals [6]. Adhesives such as fibrin or PEG hydrogel have also been tested in short gap nerve injury [7], [8]. The distinct advantage of adhesive neurorrhaphy is the lack of trauma caused by sutures, but serious issues with this technique arise in the event of a mechanical failure due to limited tensile strength [9], [10].

When extensive damage or the elastic nature of nerve tissue causes a larger gap in the fiber (> 5 mm), other approaches are usually employed, such as nerve grafts or nerve conduits. Nerve autografts have been used for over a century and are largely accepted as the gold standard treatment for large gap nerve injury today (Figure 1.7). A major concern of autografts is the inherent comorbidity of the donor nerve. Allografting avoids harvesting a similar size donor nerve, though it is generally reserved for conditions in which autografting is not a suitable treatment. After allografting, immunosuppression is necessary and the potential for serious immune response always exists [11]. The use of decellularized xenografts or allografts has also been explored, though results are often inferior to the autograft, likely due to the lack of regeneration promoting SCs in the graft [12] (Figure 1.8). Combinational approaches coupling decellularized grafts with cell therapy and neurotrophic factors is an ongoing area of research.

Nerve guidance conduits are a unique strategy for treating nerve injury that have gained significant interest both in research and clinical application. A wide variety of conduits have been designed using both natural and synthetic materials (Figure 1.9). The addition of material with the lumen, microarchitecture, neurotrophic factors, and even seeding the scaffold with autologous glial cells has further enhanced regrowth of severed axons using nerve conduits by providing a more regeneration-friendly microenvironment [13]–[15]. For example, in PNI treated with PGA conduits, victims had similar two-point discrimination as patients treated with neurorrhaphy or autologous grafting techniques in a randomized human trial [16].

Current PNI treatment, from neurorrhaphy to cell-laden nerve guidance conduits, results in variable recovery and often falls short of the “best-possible” outcomes. A study of subjects with median and ulnar neurotmesis reports satisfactory sensory recovery in less than half the cases, and motor recovery was only marginally better with 51.6% achieving satisfactory motor

function using the British Medical Research Council neurological scale [17]. A significant need exists for improved functional recovery after PNI, especially in cases of neurotmesis. Current treatments focus exclusively on reconnecting the nerve at the macro scale and rely on the unaltered regenerative abilities of peripheral neurons and SCs to regenerate functional nerves.

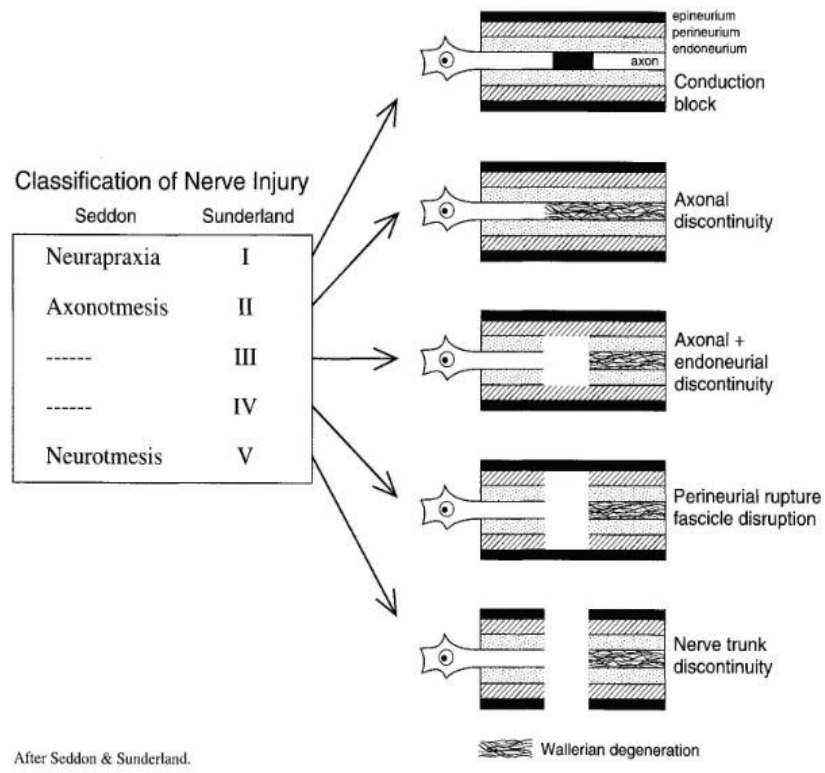


Figure 1.5 Classifications of nerve injury

The classification systems by Robert Seddon and Sydney Sunderland have considerable overlap, though Sunderland’s definition provides more detail. Used with permission. © Georg Thieme Verlag KG.

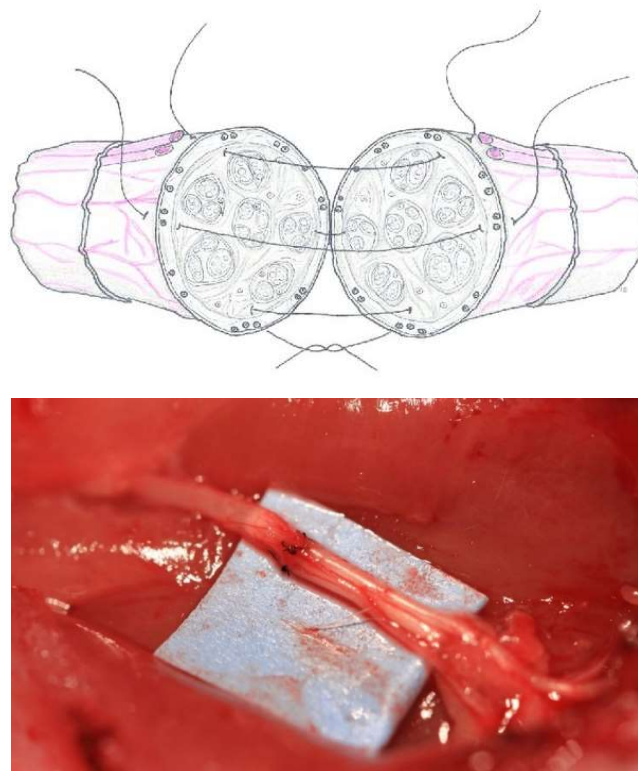


Figure 1.6 Epineurial neurorrhaphy

Neurotmesis resulting in small nerve gaps (< 5mm) may be repaired by suturing connective tissue. Top figure by Irene Espadas, lower figure “Epineurial Repair” by Jgore3, both licensed under CC BY 3.0.

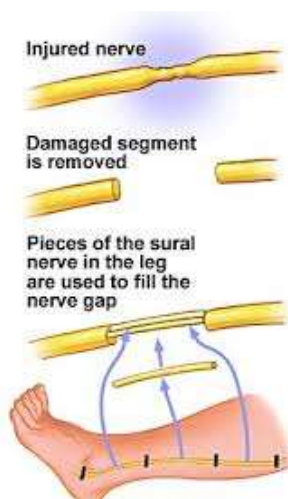


Figure 1.7 Schematic of nerve autograft

Autografts are considered the gold standard for large gap PNI but cause significant comorbidity. With permission of Mayo Foundation for Medical Education and Research, all rights reserved.

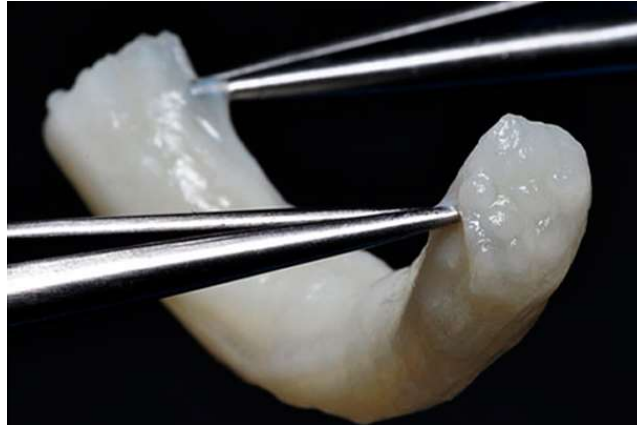


Figure 1.8 Axogen Avance nerve graft

Decellularized nerve grafts preserve native microarchitecture and extracellular matrix. Photo courtesy of Axogen Corporation.

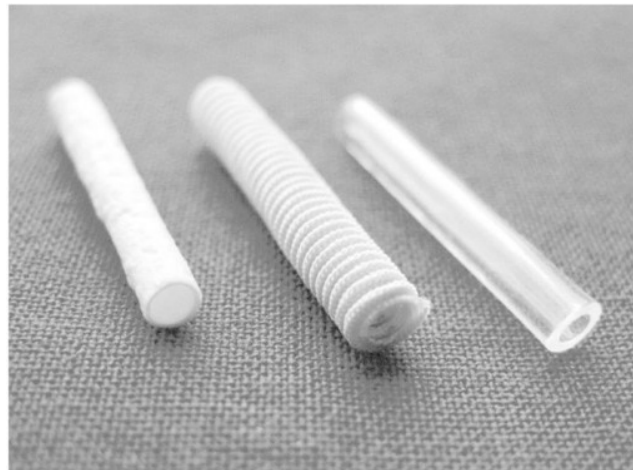


Figure 1.9 Nerve guidance conduits

Nerve guidance conduits can be made from a variety of materials including collagen, PGA and PLACL as shown here. “Nerve Conduit” published in *Regenerative Biomaterials* by Lingling Tian et al. is licensed under CC BY 3.0

1.2.2 Pathophysiology of PNI

Injuries which cause axon damage invariably lead to Wallerian degeneration (Figure 1.10). In peripheral neurons the soma is proximally located with the axon or axon-like dendrites projecting distally. An insult resulting in nerve discontinuity leads to axon breakdown distal to the site of injury because it has become separated from the soma. After injury, the proximal axon retracts from the site of damage to the nearest node of Ranvier, this response is referred to as axon dieback.

The importance of SCs in healthy nerves has already been described, however, SCs are also active participants in Wallerian degeneration and throughout nerve regeneration. Following injury, SCs are reprogrammed to a non-myelinating phenotype, also called repair SCs [18]. Repair SCs, aided by infiltrating macrophages, clear the distal nerve of debris via phagocytosis. The architecture of nerve stroma distal to the site of injury is largely preserved, thus endoneurial, perineurial, and epineurial structures become a series of hollow vascularized connective tissue tubes. In order to restore neural function, axons must cross the lesioned area, extend the length of endoneurial tubes and synapse with an appropriate target.

Regeneration of functional nerves is a highly intricate process and one which is not completely understood. Large distances, scarring, and crossing lesions are major barriers hindering axon regrowth. Aberrant regeneration, when axons regrow outside endoneurial tubes, must also be avoided. SCs aid axon regeneration through their close physical association with the neural growth cone and also supply trophic factors stimulating growth [19]. Reprogrammed repair SCs proliferate and migrate to the site of injury. Near the neural growth cone, elongated repair SCs form tracts which guide axon growth (Figure 1.11). These tracts, coined Bands of Bungner by their discoverer, extend just in front of the growth cone. The guiding presence of SCs has been suggested as a rate limiting factor in nerve regeneration and axon regrowth is rarely seen in the absence of SCs. For example, Hall showed regeneration in decellularized autografts was drastically inferior to SC-containing autografts at 2 weeks [20]. Further, Chen et al. showed by merely inhibiting SC proliferation, the number of axon profiles in the nerve bridge was reduced at 7 days post injury [21]. Torigoe et al. quantified rates of axon regrowth with respect to the presence of SCs [22]. They describe two phases of axon regrowth in injured mice, the initial phase beginning at the time of injury and lasting 2 days proceeds slowly, then after 2 days and coincident with the appearance of SCs, axon regrowth progresses nearly 4 times faster.

The guiding presence of SCs is especially important in the first stages of regrowth within the injury site, nerve graft, or guidance conduit where the native microarchitecture has been damaged. The lesioned area is the most difficult region for axons to successfully grow across and aberrant regeneration, which results in tangled or misguided axon growth, is commonly observed. Once neural growth cones enter the distal nerve, axon regrowth proceeds more successfully with the combined growth cues of SCs and the physical guidance of endoneurial tubes. The crucial growth-promoting roles of SCs makes them appealing potential targets for enhancing peripheral nerve regeneration, especially across the lesion site. One potential method for modifying SC cell behavior is the application of electrical stimulation.

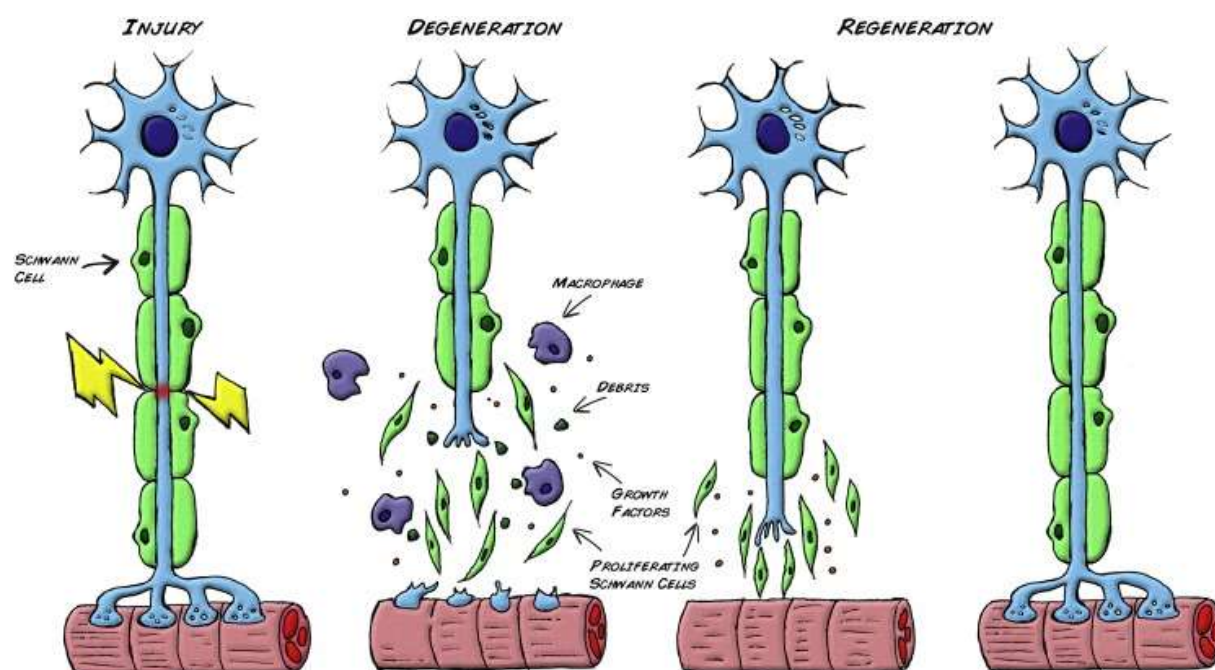


Figure 1.10 Schematic of Wallerian degeneration

After nerve injury the distal axon is broken down while the axon proximal to the site of injury remains. Macrophages and SCs phagocytose axonal and myelin debris. SCs guide the extending neural growth cone to its appropriate target. Reprinted from *Advanced Drug Delivery Reviews*, Vol 82, Alessandro Faroni et al., *Peripheral nerve regeneration: Experimental strategies and future perspectives*, 160-167, © 2015, with permission from Elsevier.

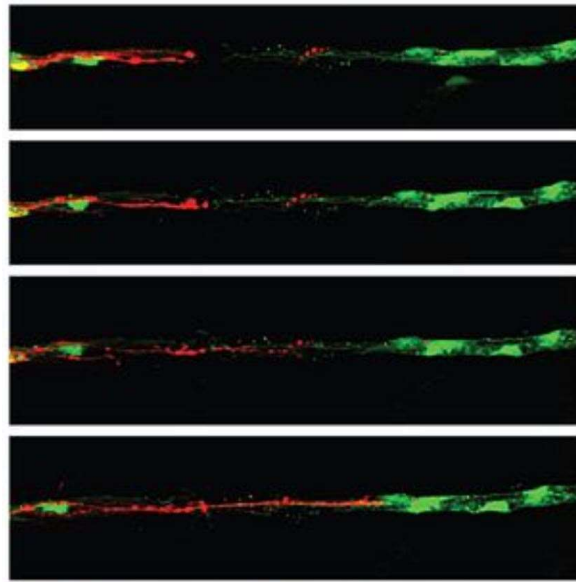


Figure 1.11 Schwann cells guiding an extending neural growth cone

After injury repair SCs guide axon regrowth by forming bands of Bungner. Here is an example of nerve regrowth in a zebrafish, SCs marked in green and neuron in red. Image by Yan Xiao et al. published in *Disease Models and Mechanisms* 2015 is licensed under CC BY 3.0.

1.3 Electric Fields

1.3.1 Endogenous Electric Fields

For hundreds of years mankind has known of electricity's potential to affect living cells. Neurons are perhaps the most famous example of bioelectricity, being able to send signals over large distances in the form of short electric pulses called action potentials. While relatively few of the body's trillions of cells are electrically excitable, studies have shown numerous cells types whose behavior is be affected by applied electric fields (EFs). At the cellular level, an EF may be thought of as a charge or voltage gradient. Charged particles exert attractive and repulsive forces on other charged particles; with the region around the particle being known as an EF.

Endogenous EFs at the tissue level have been measured in chick and xenopus (frog) embryos at various stages of development [23], [24]. These developmental fields are generated across an epithelial layer via ion pumps embedded in the membrane of the epithelial cells. The ion gradient results in a trans-epithelial potential and when holes or programmed weak points in the epithelium arise, such as the primitive streak, ions flow down their concentration gradient creating an EF [25]. Developmental EFs are transient, lasting no more than a few days before changes to the epithelial structure cuts off the flow of current. L. F. Jaffe hypothesized that endogenous EFs help establish a pattern during development [26] and significance of these EFs is underscored by the absence or malformation of entire structures when these developmental fields are disrupted [27], [28].

Beyond development, endogenous EFs have also been measured in damaged epithelium in numerous organisms, including both amphibians and mammals. A break in the epithelial layer allows ions, specifically sodium ions, to flow, and with the function of ion pumps the skin behaves like a battery. The result is a lateral EF which is thought to help direct wound repair [29]. These lateral repair EFs typically extend less than 1 mm into the undamaged epithelia and are dependent on moisture and structure of the epithelia. Examples of recorded endogenous EFs after epithelial wounds include the skin of xenopus, glabrous skin of guinea pigs, and the surface of the cornea in rats and humans amongst others [30]–[34].

1.3.2 Promoting Regeneration with Applied Electric Fields

Disruption of developmental EFs can interrupt morphogenesis, sometimes causing severe deformation of structures [27], [35]. Similarly, when endogenous EFs are disturbed after injury

wound repair is impaired [31], [36]. The potency of endogenous EFs during embryogenesis and wound repair has led to decades of experimental studies investigating the effects of applied EFs *in vitro*. Numerous studies have shown applied direct current (DC) EFs can evoke changes in cell processes, including: differentiation, proliferation, migration, neurite growth, gene expression and cell orientation [37]–[42]. The aim of applying exogenous EFs would be to provide an additional stimulus to cells within damaged tissue, creating a similar electrical environment to that present during development.

One theorized application of electrical stimulation is to enhance repair after epithelial damage by inducing cell migration. Many epithelial cells have displayed marked galvanotaxis, these include keratinocytes, epidermal stem cells, fibroblasts, and corneal cells [43]–[46]. Current medicinal practices do not include applied EF therapies for epithelial wounds; however, it is thought that appropriate EF application might enhance incomplete wound repair by enhancing cell migration.

Numerous obstacles limit nerve regeneration in the CNS, and while regrowth of peripheral nerves is better, it is also often incomplete. Because electric stimulation has marked effects on cells of the nervous system, applied EFs have been hypothesized as a potential means to improve nerve regeneration. *In vitro* studies have shown neurons exhibit aligned growth or galvanotropism when exposed to DC EFs [47], [48]. Cellular reorientation and galvanotaxis or directed migration have been observed in glial cells [42], [49], [50]. The orientation of growth and alignment as well as the direction of migration within a field appears to be dependent on at least two variables, namely, species and substratum [45], [51], [52].

Borgens et al. developed a device called the Oscillating Field Stimulator (OFS), aimed at exploiting the response of CNS neurons to applied DC EFs [53], [54] (Figure 1.12). Spinal neurons orient neurite growth parallel to an applied EF by preferentially extending neurites toward the cathode, turning existing neurites towards the cathode and sometimes reducing the growth rate or even retracting anode facing neurites [40], [55]. The OFS promotes bidirectional growth of axons within the injured spinal cord by exploiting one caveat in the response of spinal neurons – cathodal extension begins quickly after EF application, while retraction or die back of anodal neurites is delayed. By applying an oscillating DC EF which reverses polarity every 15 minutes, the cathodal axon growth is promoted before anodal retraction begins. When the polarity is reversed the phenomenon is repeated in the opposite direction and bidirectional

growth is achieved. The OFS has yielded encouraging results in paraplegic dogs as well as Phase 1 clinical trials in humans.

Following spinal injury, astrocytes form a scar at the lesion and this so-called glial scar is considered one major impediment to CNS axon regeneration. The response of cultured astrocytes (perpendicular to applied EFs) is hypothesized to facilitate spinal axon regeneration by aligning the cells within the scar in the direction of desired regrowth [42]. Taken together with the cathodal galvanotropism of spinal neurons, these are two potential mechanisms explaining the functional recovery of guinea pigs exposed to EFs after spinal cord injury [56], [57].

Peripheral neurons are naturally more capable of regeneration than their counterparts in the CNS, however, the extent of regeneration is variable and often suboptimal. Moreover, relatively little is known about the response of PNS neurons and glia to EF stimulation. To our knowledge there are no published results of DC EF stimulated neurons *in vitro* from the PNS or neural crest in mammals. *In vitro* dorsal root ganglion (DRG) and sympathetic neurons from chick embryos orient perpendicular to applied physiological EFs [48], [58]. *In vivo* conducting nerve guidance conduits with EF stimulation have been placed in the sciatic nerve of rats and have shown similar nerve regeneration to autologous grafts and were superior to the same conduit sans EF stimulation, though theories for the axon regeneration were not offered [59].

Work involving EF stimulation of SCs is also sparse. Koppes et al. have studied SC cultures as well as SC-neuron cocultures with EF stimulation. An increase in neurite outgrowth in cocultures with EF stimulation is reported, but no changes in alignment to SCs were observed [60]. In a subsequent study Koppes et al. report parallel alignment of SCs 12 hours post EF stimulation in weak fields (< 100 mV/mm) and a decrease in SC population when EFs exceeded 150 mV/mm [41]. Koppes results discord with Nguyen's findings which report perpendicular alignment of SC cultures within 6 hours of EF stimulation in fields up to 245 mV/mm [61]. Anodal SC galvanotaxis has been described by two groups [62], [63]. A more thorough characterization of SC response to EF stimulation would be useful for future application of electrical stimulation to treat PNI.

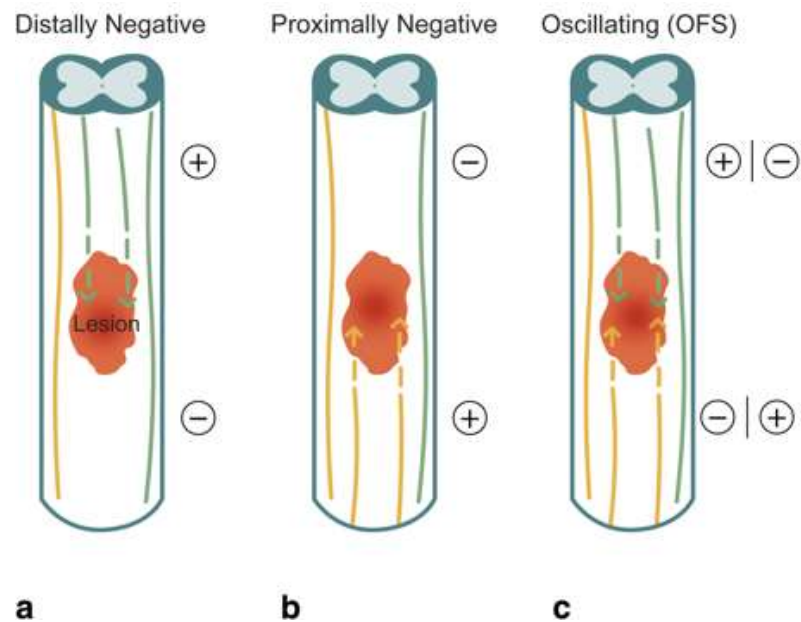


Figure 1.12 Nerve regeneration with the Oscillating Field Stimulator

The OFS utilizes cathodal galvanotropism to promote growth in both ascending and descending tracts within the spinal cord. Reprinted by permission from Springer, *Neurosurgical Review*, Weak direct current (DC) electric fields as a therapy for spinal cord injuries: review and advancement of the oscillating field stimulator (OFS) by Jianming Li, © 2018.

1.3.3 Characterizing Electric Field-Stimulated Schwann Cells to Promote Peripheral Nerve Regeneration

We've described the native regeneration promoting abilities of SCs, and the aforementioned studies by Hall, Chen, and Torigoe highlight their imperative presence for nerve regeneration, however we believe regeneration of peripheral neurons can be improved by providing cells with an additional stimulus [20]–[22]. We speculate peripheral nerve regeneration can be enhanced by augmenting the regeneration-promoting behavior of SCs or expediting the response of native SCs after injury. Electric stimulation is one noninvasive method for altering cell behavior, including cell alignment and migration. While relatively few studies have investigated the effects of electrical stimulation on SCs, we hypothesize that appropriate application of DC EFs could be used in at least two ways in the context of peripheral nerve regeneration. 1) Align repair SCs along the axis of the injured nerve, creating properly aligned Bands of Bungner and reducing aberrant growth of axons. 2) Hasten the migration of demyelinated repair SCs to the lesion site, allowing axon regrowth to begin sooner after injury. Successful application of one or both of these EF mediated responses could advance PNI treatment. In this work we aim to define SC responses to DC EFs *in vitro*, and detail methods for how these responses might be utilized in the context of PNI.

While the following experiments are performed using 2D and 3D cell culture *in vitro*, they were conducted in anticipation of future applications *in vivo*. Therapeutic electrical stimulation will require the generation of EFs in the body without creating significant side effects. A large majority of cellular EF studies utilize constant DC stimulation, which creates cytotoxic byproducts near the electrode surface. *In vitro*, cells are insulated from these byproducts by agar salt bridges. However, *in vivo* the use of salt bridges is impractical and to this end, additional stimulation regimes were tested. An oscillating waveform was tested which mimics the field created by the OFS and offers the distinct advantage of preventing the buildup of the cytotoxic species near the electrodes. Furthermore, a 50% duty cycle waveform was implemented to reduce byproduct formation rate.

The first portion of this work quantifies SC alignment, elongation and migration in 2D cell culture in response to EFs ranging from 0-500 mV/mm. In line with previous studies, constant DC stimulation was tested, as well as the more biologically relevant 50% duty cycle and oscillating DC waveforms. This proof of concept study illustrates the sensitivity of SCs to DC

EFs. The second phase of this work utilized 3D cell culture techniques to create a representative model of the microenvironment in peripheral nerves after injury. Fibrin hydrogel was selected as the matrix for the model and channel slides were created which allowed the application of 3DCC techniques. SC migration and alignment were again quantified using all three stimulation waveforms mentioned previously.

This thorough investigation of SC response to DC EFs highlights applications for electrical stimulation for PNI. Examination of variable stimulation regimes is novel and could offer insights for future research in the area of peripheral nerve regeneration.

2. APPLICATION OF ELECTRIC FIELDS TO SCHWANN CELL CULTURES

2.1 Introduction

Millions of Americans suffer from peripheral neuropathies each year, with an approximate 550,000 surgeries performed to repair nerve discontinuities created by transection injuries and promote functional recovery. As of 2009, the market for peripheral nerve repair was an estimated \$1.6 billion [1]. During peripheral nerve regrowth SCs play a key role, providing both physical and chemical guidance cues to the extending neural growth cone. The influence of SCs in nerve regeneration is accentuated by studies which have shown drastic reductions in axonal regrowth when SC populations are reduced [21], [64]. The function of repair SCs is considered a rate-limiting factor throughout peripheral nerve regeneration, therefore methods that enrich the SC's native abilities to promote axon growth are attractive targets for improving nerve regrowth and functional recovery. One innovative approach utilizes EF stimulation to enhance nerve regeneration, however, the effects of DC EFs on SCs are not well understood.

Several studies have exposed SCs to DC EFs, but none have measured EF-mediated cell alignment and migration simultaneously. One group reported no alignment during EF stimulation, and parallel cell alignment 12 hours after EF stimulation, while another reports perpendicular orientation [41], [60], [61]. In addition, two groups of researchers have shown anodal SC migration in EFs [62], [63]. Furthermore, these studies have utilized constant DC EF stimulation, and while this is a viable option *in vitro*, it is not sustainable for *in vivo* application due to the accumulation of cytotoxic byproducts. Here we concurrently evaluate SC migration, alignment, and morphology in response to physiological EFs using constant EF stimulation as well as two novel, more biologically relevant EF stimulation regimes.

2.2 Materials and Methods

2.2.1 Cell Culture

Two types of SCs were used during this study. The primary subjects were RT4 rat SCs, and culture protocols were provided by the supplier (ATCC). Basal media consisted of DMEM high glucose (Sigma) supplemented with 10% FBS (Atlanta). Penstrep media was made by

adding penicillin-streptomycin (1% v/v; 10,000 U/mL Sigma) to the basal media and only utilized to make salt bridges and for cell culture during EF experiments. SCs were expanded, aliquoted, and frozen in 10% DMSO + basal media, then placed in liquid nitrogen for long-term storage. All cells were used between passage 3–15. Cultures were passaged approximately every 3–5 days by detaching the cells from the flask with 0.25% trypsin EDTA (Sigma).

Primary SCs used for validation of RT4 SCs were obtained from the sciatic nerve of adult Sprague Dawley rats in accordance with the regulations set forth by the Purdue Animal Care and Use Committee. The method used for harvesting cells was adapted from the protocol described by Wei et al. [65]. Briefly, both sciatic nerves of deceased rats were dissected, and connective tissue removed. Segments were washed, treated with collagenase, subsequently treated with trypsin, then mechanically dissociated. After centrifugation, the nerve solution was plated and treated with media that was supplemented with cytosine-B-arabioside hydrochloride (Sigma) to inhibit fibroblast growth. Next the cultures were treated with media supplemented with human heregulin 1- β 1 extracellular domain (R&D) and SCs were separated from the remaining fibroblasts with a differential detachment step using 0.05% trypsin.

Primary fibroblasts were also harvested from the same Sprague Dawley rats, using a technique described by Seluanov et al. [66]. Briefly, 1 cm² skin fragments were excised from shaved and cleaned sites on the animals. The segments were further cut into 1 mm² fragments then placed in DMEM/F12 media (Sigma) supplemented with penicillin/streptomycin and 0.02% collagenase (Sigma) before seeding the solution on tissue culture plates.

Prior to EF stimulation SCs (RT4 or primary) were detached from cell culture flasks, centrifuged, resuspended in penstrep media and diluted to the appropriate concentration. Cell solution (100 μ L) was inserted into the channel of an IBIDI μ -slide 1 and an additional 1 mL media was added to each well. The cells were then incubated for 16 hours under standard cell culture conditions (37°C, 5% CO₂). After incubation any bubbles in the channel were removed by aspirating and returning the media from one well. Both wells were fitted with covers containing holes for salt bridges and the slide was moved into the Weatherstation climate-controlled chamber (Precision Instruments) which ensured standard cell culture conditions for the duration of experiments. Cells were exposed to EFs for 6 hours. Upon conclusion of EF stimulation, cells were promptly fixed in 4% paraformaldehyde (PF) solution (Santa Cruz Biotechnology).

2.2.2 Electric Field Setup

Electric fields were generated in the channel of the IBIDI slides using a custom-made constant current generator (John Cirillo). Each terminal of the current generator was attached to an electroplated silver/silver chloride electrode via an alligator clip. The silver/silver chloride electrodes were placed in glass vials filled with penstrep media (13 mL). Glass tubing (0.25" OD / 0.16" ID) bent into a "U" shape was filled with 2% agar in penstrep media and used as a salt bridge. One end of each salt bridge was placed in the glass vial while the other end was inserted into the well of the μ -channel slide, completing the electrolytic circuit (Figure 2.1A). Current input was monitored throughout EF experiments. Silver/silver chloride electrodes typically lasted the entirety of the experiment; however, if current input decreased, they were replaced immediately.

A reformulation of Ohm's law (Figure 2.1B) was used to calculate the current input required for the desired strength EF (E) based on the known parameters of conductivity ($\sigma = 0.001603 \text{ ohm}^{-1} \text{ mm}^{-1}$), current (I) and cross-sectional area of the channel ($A = 2 \text{ mm}^2$). A finite element analysis model of the EF generated was created using Sim4Life simulation software and geometries of the IBIDI channel slide. The model predicts a uniform EF across the length of the channel (Figure 2.1). Additionally, the Sim4Life model and calculation were verified by manually measuring the voltage at either end of the channel and dividing the measured voltage by the length of the channel, giving the value of the EF (mV/mm).

EFs conditions were defined by the field strength and DC stimulation waveform. Five EF strengths were tested 0 mV/mm (0 mA), 10 mV/mm (0.03 mA), 75 mV/mm (0.16 mA), 200 mV/mm (0.24 mA) and 500 mV/mm (0.64 mA). The three DC waveforms which were tested were constant DC (Con), 50% duty cycle DC (50% dc), and oscillating DC (Osc) (Figure 2.2). The latter two waveforms were created by connecting the leads from the current generator to a switch which had two settings: 1) 50% duty cycle - turned the current on/off in 15-minute intervals or 2) oscillating - reversed the polarity of the current every 15 minutes.

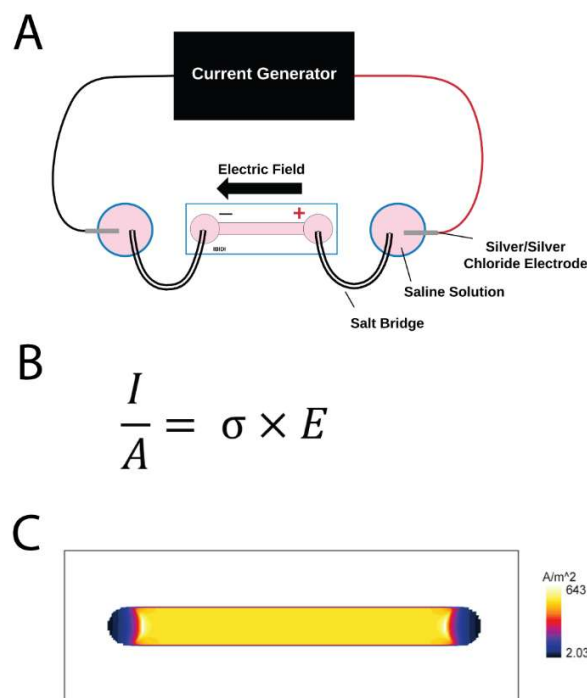


Figure 2.1 Electric field setup, calculation, and model

(A) Diagram of electrolytic circuit generating an electric field in the cell chamber. A custom current generator, wiring, agar salt bridges and an IBIDI μ -Channel slide 1 were used to create a uniform electric field.** (B) Reformation of Ohm's Law used to calculate the electric field in the channel, where I = current (adjustable - determined by constant current generator), A = cross sectional area of the channel, σ = conductivity and E = electric field (C) Finite element analysis model of a constant DC electric field generated across the channel of an IBIDI slide. As DC current was supplied, the Sim4Life Ohmic Quasi-Static EM Low Frequency solver was used to solve electric fields and current densities. Conductivity of the cell media was measured, and geometries of the slide were supplied by the manufacturer.

***Please note figures 2.1-2.16 were adapted and reprinted with permission from Springer. Annals of Biomedical Engineering, "DC Electric Fields Induce Perpendicular Alignment and Enhanced Migration in Schwann Cell Cultures", S. J. Bunn, A. Lai, and J. Li © 2019.*

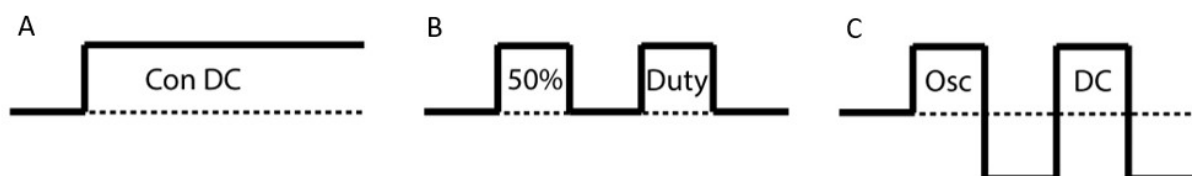


Figure 2.2 DC electric field stimulation regimes

Three distinct waveforms were used for DC EF stimulation (A) constant, (B) 50% duty cycle (15 minutes on / 15 minutes off) and (C) oscillating (polarity reversed every 15 minutes).**

2.2.3 Migration Tracking

SC migration was tracked through analysis of phase contrast time-lapse images (Figure 2.3). Automated image collection (1 image/minute) was performed using Metamorph Premier Version 7.7.4.0 (Molecular Devices) with an Olympus IX81 microscope and an EXi Blue camera (QImaging). Once experiments were completed, an image sequence of every 10th image was loaded into FIJI (National Institutes of Health, version 1.52n). The center of each cell which remained in the field of view for the duration of the experiment was tracked using the Manual Tracking plugin. The data was used to calculate three measures of cell migration: X-displacement, Y-displacement and distance. X- and Y-displacement were defined as the starting X/Y coordinate minus the final X/Y coordinate. Distance was defined as the total path the cell travelled and was calculated as the sum of the linear distances between each frame, thus distance was always equal to or greater than either X- or Y-displacement. Time-lapse videos were rendered to show the response of cells to the various EFs tested.

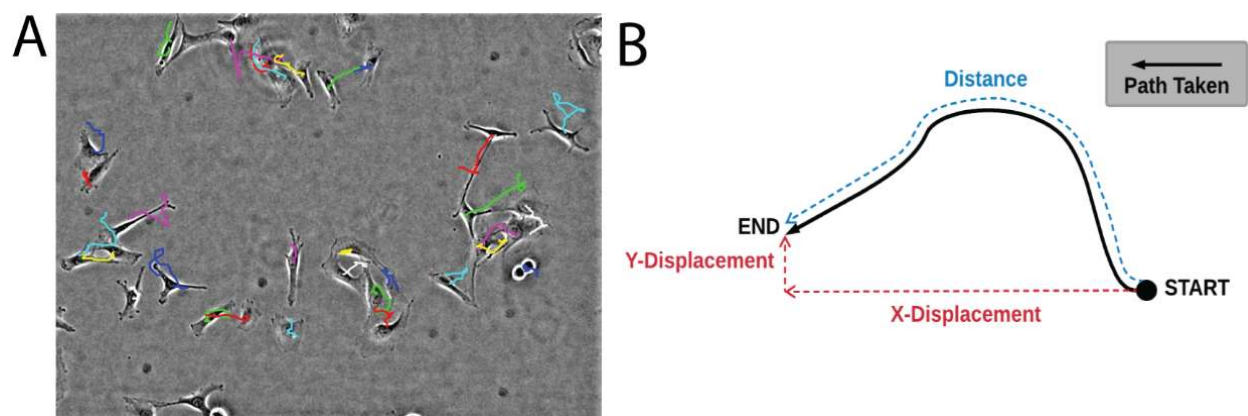


Figure 2.3 Schwann cell migration tracking

(A) Trace of SC paths (colored lines) overlaid on time-lapse images of SCs during EF stimulation. (B) Definitions of distance, X-displacement, and Y-displacement.**

2.2.4 Proliferation Rate & Angle of Cell Division

Time-lapse images recorded during EF exposure were also used to assess SC proliferation rates and angle of cell division. Proliferation rate was quantified by counting the number of cell divisions within the field of view and dividing by the initial number of cells. The

angle of cell division was quantified by measuring the angle created by a line between the centers of each daughter cell in the first image where the daughter cells were separate entities (Figure 2.4).

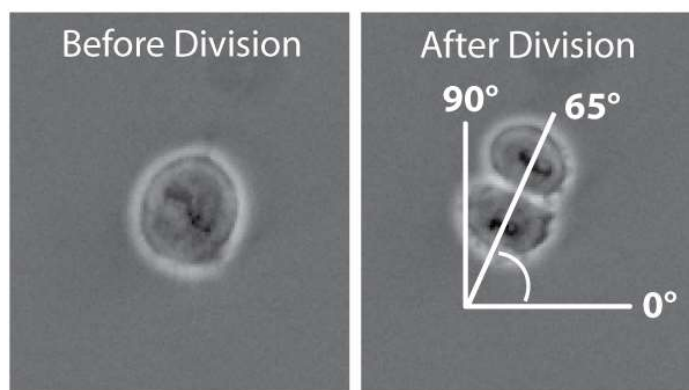


Figure 2.4 Angle of cell division schematic

Angle of cell division is the orientation of the line drawn between the center of two daughter cells with respect to the electric field vector.

2.2.5 Alignment & Morphology

SC alignment and morphology was measured from fluorescent images of fixed cells after EF stimulation. Triton X-100 was used to permeabilize cells (5 minutes) then the cells were rinsed three times with PBS. Next the nucleus was stained using propidium iodide (Invitrogen; 0.05 mg/mL) or 4',6-diamidino-2-phenylindole (DAPI) (Biotium; 300 nM) and actin was stained using Alexa Fluor 488 Phalloidin (Invitrogen; 1:50). Unbound stain was removed by washing cells in PBS three times (5 minutes), then cells were imaged using the same microscope and mercury vapor fluorescent light source (X-cite).

Cell alignment was approximated by the alignment of the cell nuclei. Fluorescent images were loaded into FIJI and a macro was used to quantify the alignment of each nucleus (Figure 2.5). The macro utilized the “autothreshold” command with the “minimum dark” setting. The threshold value was adjusted based on the brightness of the images. After thresholding the macro created a best fit ellipse for each object larger than 200 square pixels. The angle of the large axis of each ellipse was used as in cell alignment data. Nuclei which bordered the edge of the image or overlapped another nucleus were discarded or corrected. Images were captured with the EF

vector oriented along the X-axis, thus cells which had an angle of 0° were oriented parallel to the EF while cells with an angle of 90° were perpendicular. As cells have no true “front” or “back”, the angles measured in FIJI (0-180°) were mirrored about the Y-axis so all alignment data is reported from 0-90°. Cells oriented between 80-90° were considered to be “near-perpendicular”.

Cell morphology was quantified through analysis of images of the cell actin cytoskeleton in NIS Elements AR Version 5.02.00. The automated measurement tool was used to identify and measure elongation of isolated cells. Elongation was defined as the ratio of max feret/min feret, with a perfectly circular cell having an elongation of 1 and more bipolar cells having larger elongation values. Measurements from overlapping or partial cells were discarded.

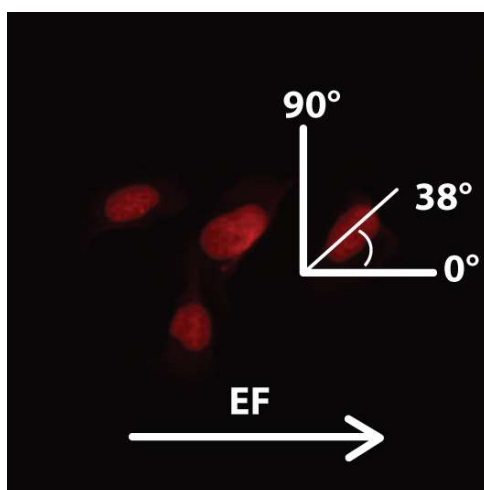


Figure 2.5 Cell alignment schematic

The angle between the long axis of cell nuclei and the EF vector (horizontal) was defined as the angle of cell alignment.**

2.2.6 Immunofluorescence

Immunofluorescence of S100 protein was used to assess the purity of primary cell cultures. Fixed primary SCs and fibroblasts were permeabilized using 0.1% Triton X-100 (5 minutes), then anti-S100 primary antibody (Thermo-Fisher) was added (1:100) and left at room temperature for 30 minutes, then stored at 4°C overnight. The following day the primary antibody solution was aspirated, and the cells were washed thrice with 0.1% Tween 20 (Sigma) for 10 minutes. After washing, a blocking solution containing 5% FBS in 0.1% Tween 20 was

added for 1 hour. The blocking solution was aspirated, and the cells were gently rinsed one time with 0.1% Tween 20 solution. Alexa Fluor goat anti-mouse secondary antibody in 0.1% Tween 20 was added (Jackson ImmunoResearch; 1:1000) for 1 hour. After aspirating the secondary antibody, the cells were washed with 0.1% Tween 20 solution three times (10 minutes). Cells were bathed in PBS solution for fluorescent imaging. Ten images of both primary SCs and primary fibroblasts were collected then loaded into FIJI. The ROIs were the outlines of the cells, defined by thresholding, then the intensity of the pixels within the ROI were measured. From the mean pixel intensity values a cutoff was established for determining SCs or fibroblasts.

Immunofluorescence of Integrin $\beta 1$ ($I\beta 1$) was performed to investigate the possibility of a re-arrangement of the protein in response to EF exposure. SCs were fixed, permeabilized and rinsed as before. Anti-integrin $\beta 1$ primary antibody in PBS (EMD Millipore; 1:100) was added and left at room temperature for 30 minutes then stored at 4°C overnight. Next the cells were washed with three times with 0.1% Tween 20 (10 minutes), then blocking solution was added for 1 hour. Alexa Fluor 488 labelled secondary antibody (1:1000) in 0.1% Tween 20 was then added for 1 hour. Finally, cells were washed in 0.1% Tween 20 three times before imaging.

2.2.7 Statistical Analysis

Trials for all EF conditions were performed in triplicate. Statistical analysis was performed on migration data (distance, X-displacement and Y-displacement), angle of cell alignment and elongation. The significance level for all tests was $\alpha = 0.05$. Analysis of Con EF distance was evaluated using ANOVA with a Bonferroni post hoc test. All other data were nonparametric and a Kruskal Wallis test with a Bonferroni post hoc test was used.

2.3 Results

2.3.1 Migration

Minimal directed SC migration was observed during 6-hour EF exposures with one exception – SCs exposed to 500 mV/mm Con EFs showed some directional bias with mean X-displacement of 7.5 $\mu\text{m/hr}$ toward the cathode. Several other EF conditions were found to have X- and Y-displacements statistically different than controls, however the magnitudes of these displacements were very small. EF exposure appeared to have some influence on cell motility causing cells exposed to higher strength EFs to have larger path lengths.

2.3.1.1 Constant EFs

Mean SC X-displacement in Con EFs were near 0 μm for all field strengths except 500 mV/mm, though 10 and 75 mV/mm were also statistically different than the control group ($p < 0.05$; $p < 0.001$) (Figure 2.6A). Control SCs (0 mV/mm) had a mean X-displacement of $3.0 \pm 42.7 \mu\text{m}$ toward the cathode, while SCs in 500 mV/mm had a mean X-displacement of $45.0 \pm 60.4 \mu\text{m}$ toward the cathode ($p < 0.001$). The mean Y-displacement of the control group as well as all EF strengths tested were near 0 μm , though the mean of SCs exposed to 200 mV/mm was statistically different ($p < 0.05$) (Figure 2.6B). EF exposure led to larger distances travelled at all field strengths except 75 mV/mm which was not statistically significant ($p > 0.05$) (Figure 2.6C). Control SCs had a mean distance of $115.9 \pm 51.0 \mu\text{m}$ while SCs in 500 mV/mm EFs had a mean distance of 170.8 ± 68.7 , a 47% increase in distance travelled.

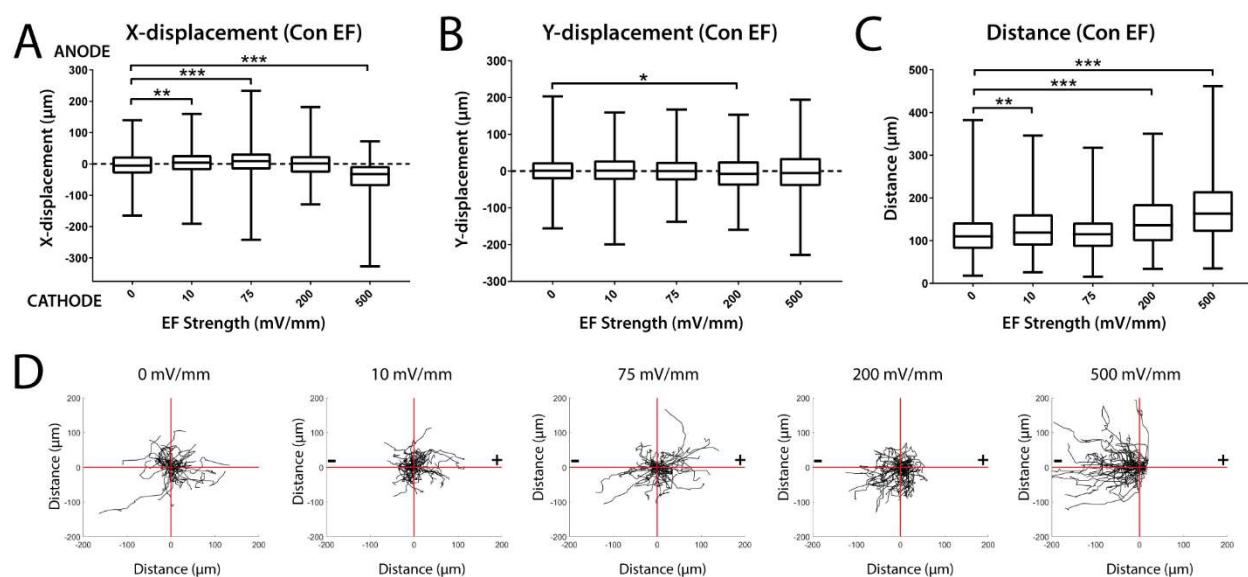


Figure 2.6 Migration in constant electric fields

SC (A) X-displacement (B) Y-displacement and (C) distance during 6-hour Con EF exposure. (D) Plots of cell migration path ($n = 50$).**

2.3.1.2 50% Duty Cycle EFs

In 50% d.c. EFs SCs in all field strengths had X-displacements which were statistically different from controls (10 mV/mm $p < 0.01$, 75 mV/mm $p < 0.01$, 200 mV/mm $p < 0.001$, 500 mV/mm $p < 0.001$), with slight bias toward the anode (Figure 2.7A). Y-displacement of SCs was

not statistically different than controls for any EF strength (Figure 2.7B). The mean distance travelled increased for SCs exposed to 200 and 500 mV/mm d.c. EFs ($p < 0.001$, $p < 0.01$) (Figure 2.7C).

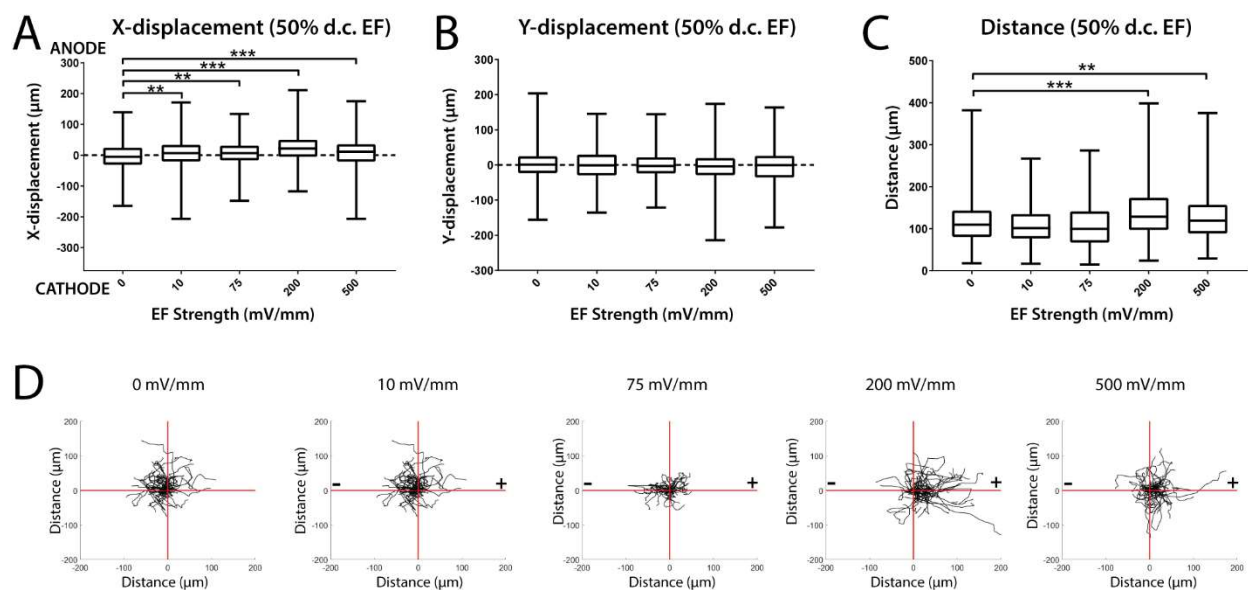


Figure 2.7 Migration in 50% duty cycle electric fields

SC (A) X-displacement (B) Y-displacement and (C) distance during 6-hour duty cycle EF exposure. (D) Plots of migration path of 50 cells for each field strength tested.*

2.3.1.3 Oscillating EFs

Little X- or Y-displacement was observed in SCs exposed to Osc EFs, although SCs exposed to 75 mV/mm had statistically significant X-displacement ($p < 0.01$) and SCs in 10 mV/mm had statistically significant Y-displacement (Figure 2.8A & B). The mean distance travelled was increased in 10, 200 and 500 mV/mm Osc EFs ($p < 0.001$ for each) (Figure 2.8C).

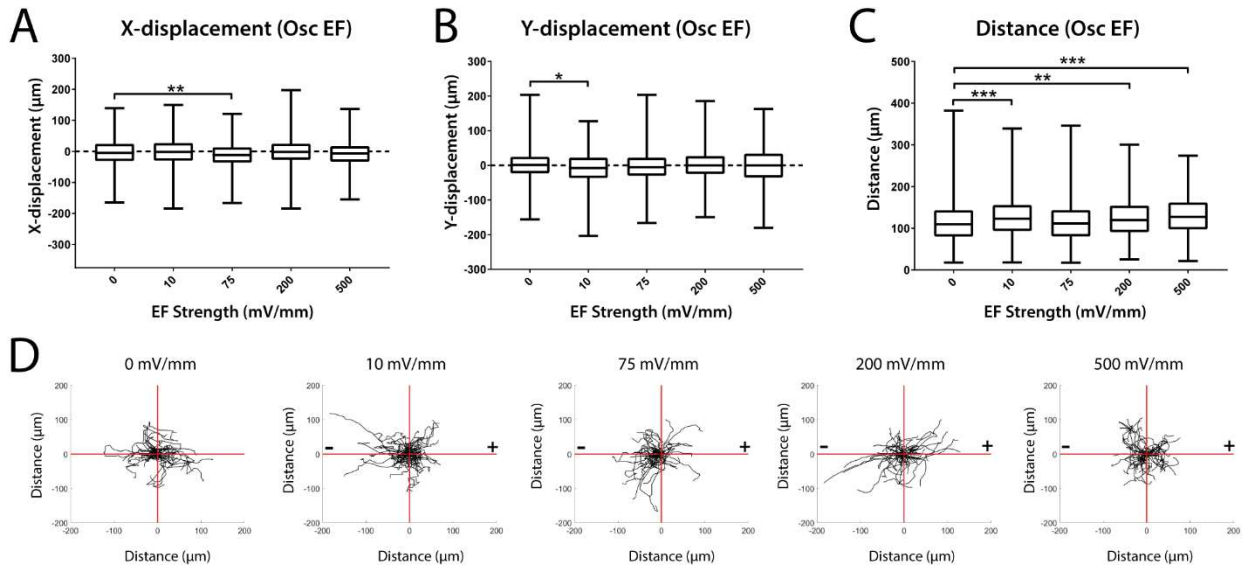


Figure 2.8 Migration in oscillating electric fields

SC (A) X-displacement (B) Y-displacement and (C) distance during 6-hour Osc EF exposure. (D) Plots of migration path of 50 cells for each field strength tested.*

2.3.2 Proliferation Rate

No significant changes in proliferation rate were observed in SCs exposed to EFs of any field strength or waveform compared with controls ($p > 0.05$) (Figure 2.9A-C). Proliferation rate of SCs was highly variable among trials, ranging from 19.8 – 49.1%.

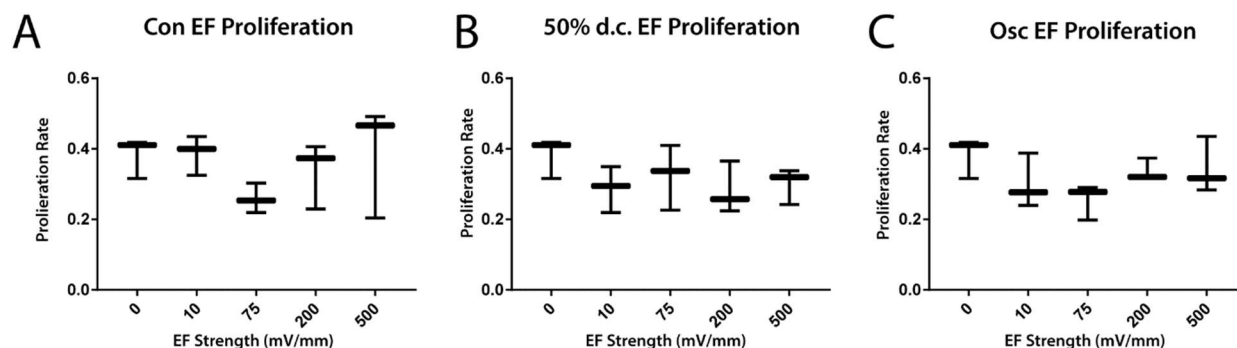


Figure 2.9 Schwann cell proliferation in electric fields

No significant changes in SC proliferation over 6 hours were observed in **(A)** Con EFs, **(B)** 50% d.c. EFs or **(C)** Osc EFs.

2.3.3 Angle of Cell Division

The angle of cell division was influenced by the application of exogenous EFs (Figure 2.10A-C). Daughter cells tended to align perpendicular to the EF vector. Significant bias in the angle of cell division was observed in 200 and 500 mV/mm Con EFs ($p < 0.001$ for both), 200 and 500 mV/mm d.c. EFs ($p < 0.05$, $p < 0.001$) and 500 mV/mm Osc EFs ($p < 0.001$). The greatest alignment was observed in 500 mV/mm Con EFs with a mean angle of cell division of $64.9 \pm 22.1^\circ$. Control SCs had a mean angle of cell division of $43.5 \pm 25.7^\circ$.

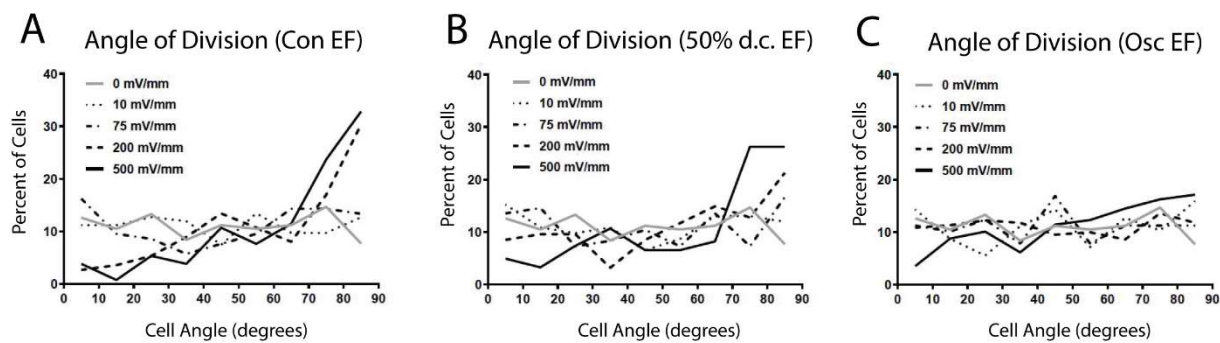


Figure 2.10 Angle of cell division

High strength EFs induce oriented cell division in (A) Con, (B) 50% d.c., and (C) Osc EFs. **

2.3.4 Alignment

EF exposure induced perpendicular alignment of SCs. The extent of alignment was dependent upon EF strength as well as the stimulation regime. Con EFs were shown to induce the greatest cell alignment of the three DC stimulation waveforms tested. Field strengths as low as 75 mV/mm were shown to induce significant perpendicular alignment.

2.3.4.1 Con EFs

Con EF induced perpendicular alignment in SCs exposed to EFs of 75 mV/mm and greater (Figure 2.11A). Perpendicular alignment increased with EF strength: control SCs had a mean cell angle of $45.3 \pm 26.1^\circ$ while SCs exposed to EFs had mean cell angles of $46.9 \pm 25.7^\circ$ (10 mV/mm), $49.2 \pm 26.1^\circ$ (75 mV/mm), $61.6 \pm 22.6^\circ$ (200 mV/mm) and $69.9 \pm 19.0^\circ$ (500 mV/mm). Over 39% of SCs exposed to 500 mV/mm EFs had near-perpendicular alignment as compared to 10.7% of control SCs.

2.3.4.2 50% d.c. EFs

Perpendicular alignment was also observed in 50% d.c. EFs, though the mean cell angles and percentage of cells with near perpendicular alignment were reduced compared with Con EFs (Figure 2.11B). 75 ($46.0 \pm 26.4^\circ$), 200 ($53.4 \pm 25.4^\circ$) and 500 mV/mm ($63.4 \pm 22.4^\circ$) EFs had mean cell alignment that was statistically greater than controls ($p < 0.01$, $p < 0.001$, $p < 0.001$). Near-perpendicular alignment was seen in 27.6% of cells in 500 mV/mm EFs.

2.3.4.3 Osc EFs

Oscillating fields induced significant perpendicular alignment of SCs only in the highest field strength ($p < 0.001$) (Figure 2.11C). The mean cell angle of SCs exposed to 500 mV/mm Osc EFs was $54.3 \pm 25.4^\circ$, while the other field strengths tested had mean cell angles very close to the control group ($45.3 \pm 26.1^\circ$). Near-perpendicular alignment was observed in 18.3% of SCs exposed to 500 mV/mm Osc EFs.

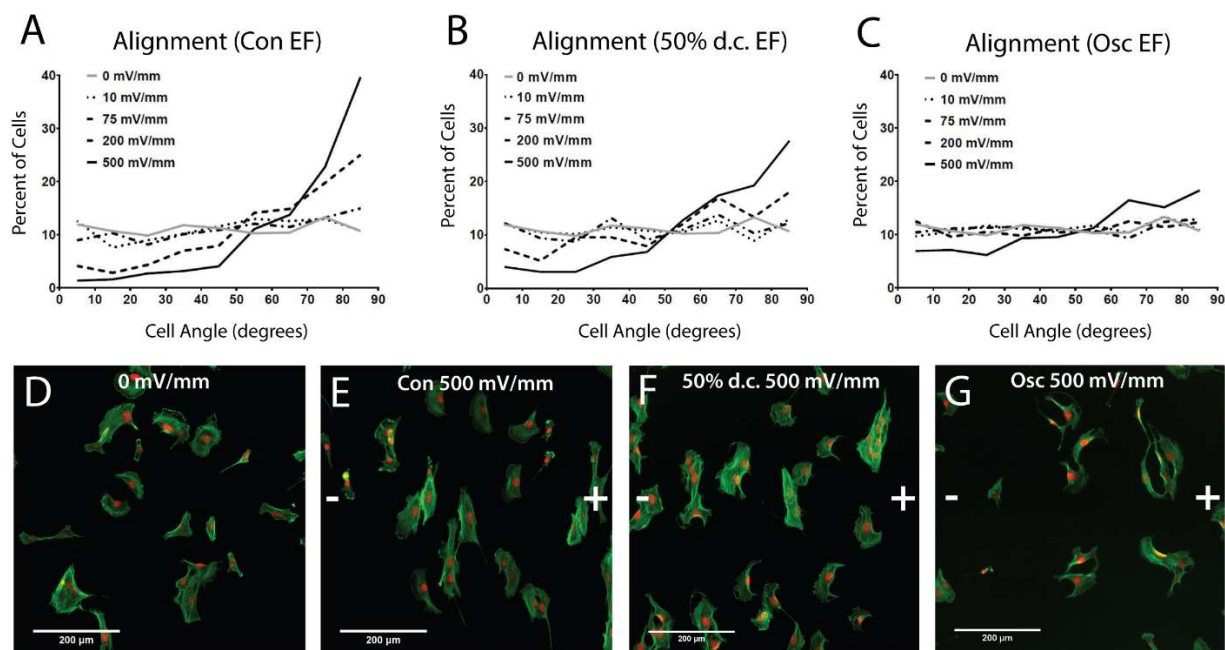


Figure 2.11 Schwann cell alignment in electric fields

Perpendicular SC alignment was observed in **(A)** Con EFs, **(B)** 50% d.c. EFs and **(C)** Osc EFs. **(D-G)** Representative fluorescent images showing actin in green and nucleus in red. Scale bar 200 μm .**

Table 1 Schwann cell alignment data in 2D

Electric Field Condition (mV/mm)	Mean Angle (\pm std dev)	Percent $\geq 80^\circ$	
Control	0	$45.3 \pm 26.1^\circ$	10.7%
Constant EF	10	$46.9 \pm 25.7^\circ$	10.8%
	75	$49.2 \pm 26.1^\circ$	15.0%
	200	$61.6 \pm 22.6^\circ$	25.2%
	500	$69.9 \pm 19.0^\circ$	39.6%
50% Duty Cycle EF	10	$44.5 \pm 25.9^\circ$	11.0%
	75	$45.6 \pm 25.6^\circ$	10.1%
	200	$53.1 \pm 25.3^\circ$	17.6%
	500	$62.1 \pm 22.5^\circ$	24.2%
Oscillating EF	10	$46.0 \pm 25.8^\circ$	10.9%
	75	$46.0 \pm 26.2^\circ$	12.9%
	200	$46.1 \pm 26.5^\circ$	12.3%
	500	$54.3 \pm 25.4^\circ$	18.3%

2.3.5 Morphology

SC morphology became more bipolar with EF exposure (Figure 2.12A-C). Significant changes in elongation were observed in 500 mV/mm Con and Osc EFs ($p < 0.001$, $p < 0.01$). The control group had a mean elongation of 1.93 ± 0.63 while SCs exposed to 500 mV/mm Con EFs had a mean elongation of 2.56 ± 0.97 and SCs exposed to 500 mV/mm Osc EFs had a mean elongation of 2.28 ± 0.71 .

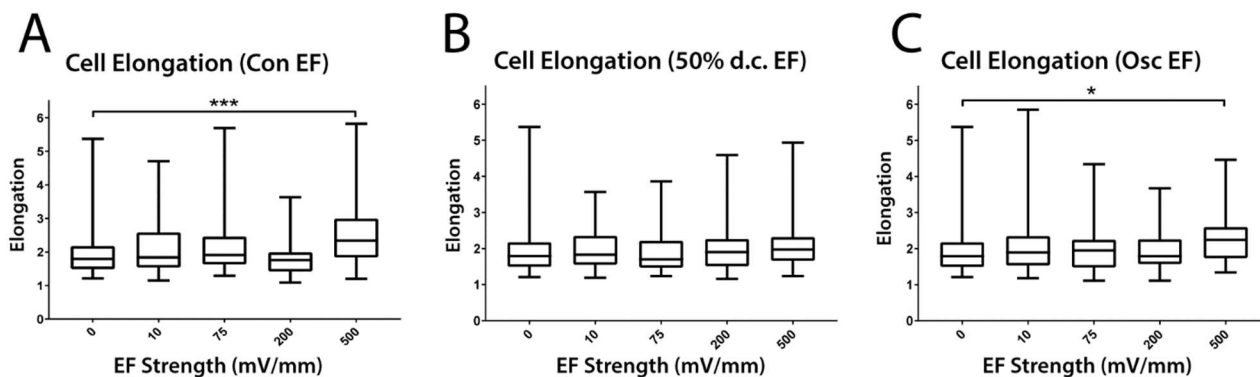


Figure 2.12 Schwann cell elongation

SCs exposed to 500 mV/mm Con and Osc EFs had a significantly more elongated morphology compared with unstimulated SCs ($p < 0.001$, $p < 0.01$).**

2.3.6 Primary Schwann Cell Comparison

Primary SCs expressed greater amounts of S100 protein than primary fibroblasts (Figure 2.13) ($p < 0.01$). Primary SCs had a mean pixel intensity of 25.0 ± 3.50 while primary fibroblasts had a mean pixel intensity of 19.8 ± 0.62 . Cells with a mean pixel intensity value greater than 21 were classified as SCs, while those with mean pixel intensities less than 21 were considered fibroblasts. Utilizing this definition of cell type, our primary cultures consisted of 96% SCs. Primary SC cultures exposed to EFs were found to behave similarly to RT4 SCs (Figure 2.14). Primary SCs cultures were more motile than RT4 cultures with and without electrical stimulation. The perpendicular reorientation of SCs was observed in similar degree in both cell types.

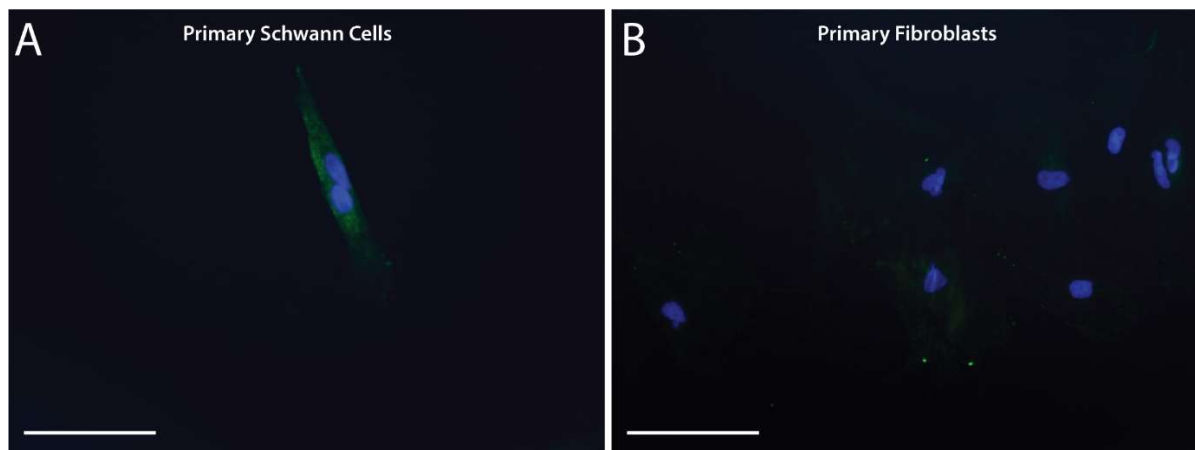


Figure 2.13 S100 protein expression in primary Schwann cells

S100 is a protein typically expressed in cells derived from the neural crest. **(A)** Primary SCs had an elevated S100 protein expression compared with **(B)** primary fibroblasts taken from the skin of Sprague Dawley rats. S100 shown in green. DAPI shown in blue. Scale bar 50 μm .

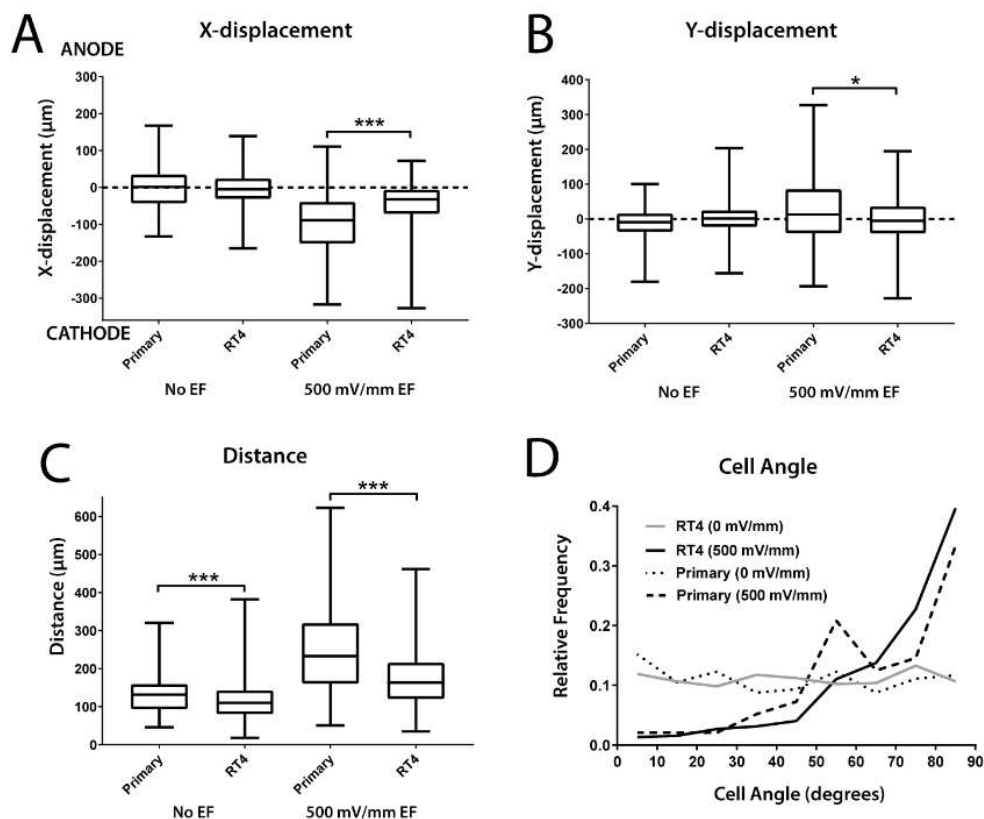


Figure 2.14 Migration and alignment of primary Schwann cells

(A-C) Primary SCs were more motile with and without EF stimulation. The direction of galvanotaxis and **(D)** perpendicular orientation was similar in both cell types.**

2.3.7 Integrin β 1 Distribution

Immunofluorescence of controls and SCs exposed to 500 mV/mm Con EFs revealed no intracellular asymmetry of I β 1 (Figure 2.15). The I β 1 staining was diffuse and located throughout the cytoplasm in EF stimulated and unstimulated SCs. No bias toward either the anode or cathode-facing sides of the cells was observed.

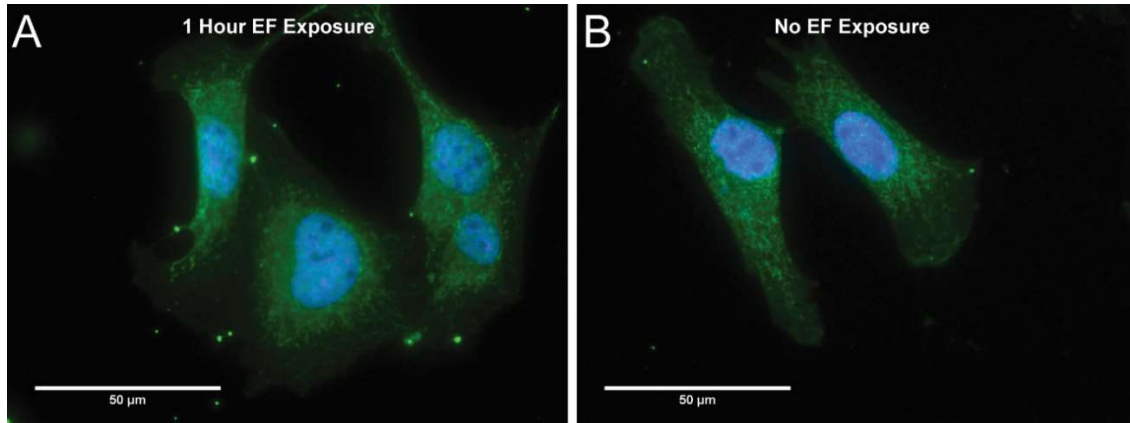


Figure 2.15 Integrin β 1 expression in Schwann cells

Intracellular distribution of I β 1 was similar in **(A)** EF stimulated and **(B)** unstimulated SCs. No bias in I β 1 distribution was observed in SCs exposed for 15 min, 30 min, 1 hr, 3 hrs or 6 hrs. Scale bar 50 μ m.**

2.4 Discussion

In this work, effects of DC EF stimulation regimes on RT4 SC behavior, including alignment, morphology, and migration, were evaluated. The motivating hypothesis driving this study is the application of EFs to control cell behavior, in this case, alter SCs to enhance axon regrowth after injury. The stimulation regimes tested included constant DC, 50% duty cycle DC, and oscillating DC. The vast majority of cellular studies of EF stimulation use a constant stimulation waveform. Constant DC EF stimulation is easily adapted to *in vitro* experiments with the use of salt bridges, which insulate cell cultures from the toxic byproducts, however, its' significance *in vivo* can be questioned. Two alternate stimulation waveforms were tested in this study – 50% duty cycle DC and oscillating DC, both with 15 min cycle intervals. Rationale for use of a duty cycle stimulation waveform includes promoting a unidirectional cell response, decreasing power requirements/byproduct production and allowing more time for byproduct removal, additionally a comparable stimulation regime was implemented successfully in injured cat spinal cords [67]. The idea of an oscillating DC waveform was taken from the Oscillating Field Stimulator (OFS) an implantable device developed by Borgens et al. for promoting bidirectional regrowth of spinal neurons [53], [54]. The oscillating DC waveform provides the additional benefit of preventing the buildup of EF byproducts at the electrodes. All three stimulation regimes were tested at various physiologically relevant EF strengths, ranging from 10-500 mV/mm (Shi and Borgens 1994)[35]. These field strengths are in line with previous EF stimulation experiments involving SCs and neurons [41], [62], [68].

Of the cell behaviors examined in this study, cell alignment was most noticeably affected by EF stimulation. SCs displayed readily apparent perpendicular alignment at high (500 mV/mm) field strengths, and significant alignment was detected in field strengths as low as 75 mV/mm (Figure 2.11A). While all experiments were conducted over a 6-hour period, SC reorientation could be observed quickly (less than 1 hour) in 500 mV/mm EFs. The short timeframe of cellular perpendicular alignment agrees with studies investigating fibroblast migration in EFs [51]. The orientation of the alignment perpendicular to the EF concurs with findings of other cells originating from the ectoderm including fibroblasts and astrocytes [42], [51]. Previous studies of EF-mediated SC alignment did not observe perpendicular alignment during stimulation at field strength up to 200 mV/mm, however at 12 hours post-stimulation they reported parallel cell alignment [41], [60]. One noted discrepancy in the experimental setup

between the current study and that performed by Koppes et al. was the seeding density. The significantly higher seeding density used by Koppes et al. may have led to more cell to cell interactions and a diminished alignment response. Another incongruity between the two studies was the charge of cell culture surface. Koppes et al. coated glass slides with poly-L-lysine (PLL) giving the surface a net positive charge, while this work used a proprietary polycarbonate slide with a net negative charge. Consistency of the substrate is a very important detail; Rajnicek et al. showed the direction of galvanotropism could be altered with changes in surface charge [52]. To investigate effects of surface charge on SC response to EF stimulation, we conducted experiments using PLL surfaces (Figure 2.16). In 500 mV/mm Con EFs, SCs displayed similar alignment responses on uncoated and PLL coated slides (Figure 2.16D). Additional experiments were conducted to investigate the effect of varying cell density on cell alignment. The densities tested ranged from primarily isolated cells (2,000 cell/cm²) to nearly confluent (16,000 cell/cm²). Mean cell alignment increased with increasing cell densities. The greatest perpendicular alignment observed in 500 mV/mm Con EFs (16,000 cell/cm²) had a mean cell angle of $69.5 \pm 20.2^\circ$ with 39.4% having near-perpendicular alignment.

High strength (500 mV/mm) continuous (Con and Osc) EF stimulation was shown to significantly affect cell morphology, causing SCs to become more elongated (Figure 2.12). Morphology was quantified by measuring the elongation (ratio of max feret/min feret) of the actin cytoskeleton. While previous studies have not quantified changes in cell morphology, a similar response is observed in fibroblasts and Yao et al. report upregulation of the PKN3 gene in SCs after EF stimulation, a gene known to influence morphology in endothelial cells [51], [62], [69].

While not as obvious as the alignment response, we found that SC migration was also affected by EF stimulation. In 500 mV/mm Con EF there was notable cathodal galvanotaxis (negative pole); these cells had an average X-displacement of 7.5 $\mu\text{m/hr}$ (Figure 2.6A). Even in weaker EF conditions which did not lead to discernable galvanotaxis, there was a trend toward increased overall cell motility with EF stimulation (Figures 2.6-2.8). Two earlier studies investigated SC migration in EFs and reported anodal movement [62], [63]. The current findings differ from these published results, and while the differences may not be fully explained, a number of important differences exist. The study conducted by McKasson et al. utilized embryonic SCs harvested from chick ganglia, and previous studies have shown EF-mediated

responses can be species dependent. For example, fibroblasts from humans and quail have been shown to migrate in opposite directions [45], [51]. Substratum effects on cell growth have already been described, thus it is important to note the EF chambers used by McKasson et al. were coated with laminin and those used by Yao et al. were coated with laminin and PLL. While a laminin coating likely led to an overall negative surface charge (IBIDI channel slides also had a negative charge per communications with the manufacturer), Rajnicek et al. found neurons cultured on laminin and laminin + PLL had diminished growth compared to neurons grown on Falcon plastic. Galvanotaxis of SCs on PLL coated IBIDI slides was negligible (Figure 2.16A). Substrate and species are variables which might explain the differences in SC migration and these factors must be considered in future applications of EF stimulation *in vivo*.

EF stimulation regime impacted SCs, with Con EFs inducing the most evident changes in migration, alignment, and morphology. When cell alignment is plotted by stimulation regime, the reduction in cell alignment in 50% d.c. and Osc EFs becomes evident (Figure 2.17). Although the duty cycle stimulation regime exposes cells to EFs for only half of an experiment duration, it still induced a greater response than continuous electrical stimulation in an oscillating waveform.

Electrical stimulation has been convincingly shown to influence number of cell behaviors, but debates surrounding the signal transduction mechanism(s) are ongoing. One popular hypothesis involves the polarization of charged membrane proteins either by electrophoresis or electro-osmotic flow. Models and experimental data support the concept of membrane bound protein movement in response to EFs, but whether this protein localization is responsible for cell polarization needs further confirmation [70]–[72]. Direct effects of EFs on a cell's transmembrane potential has also been suggested as a polarizing mechanism. It is thought that asymmetrical transmembrane potentials across a cell could polarize the cell by creating depolarized and hyperpolarized regions at the extremes. The inhomogeneity of transmembrane potential across the length of the cell lead to variable ion channel activity, especially voltage-gated channels, which then affect a host of intracellular signaling cascades [72]. This mechanism of polarization would have a bias toward larger cells, as there would be a greater difference in transmembrane potential.

Integrins are ECM binding proteins which have been suggested as a potential EF-sensing molecule, to explore this possibility in SCs we examined integrin $\beta 1$ (IB1) expression in electrically stimulated SCs [73]. While cells in 500 mV/mm Con EFs showed profound cell

polarization and slight cathodal migration, no asymmetric redistribution of IB1 was observed (Figure 2.15).

With the large volume of cells required for the study's completion, the RT4 cell line was used as a proxy for primary SCs. Use of an immortal cell line obviously raises questions of relevancy of the findings to primary cells. For this reason, RT4 cell line use was verified with a direct comparison to primary SCs. Unsurprisingly, both RT4 and primary SCs exhibited similar responses to EF stimulation. Under control conditions as well as with EF stimulation, primary SCs were found to be more motile than RT4 SCs ($p < 0.001$ for both). While cathodal migration was observed in both RT4 and primary SCs, the primary cells migrated larger distances toward the cathode ($p < 0.001$). With discrepancies in overall cell motility noted, RT4 SCs appear to be an appropriate model for evaluating SC response to EF stimulation.

The identity of cells harvested from rat sciatic nerve was verified using S100 immunofluorescence. S100 is a family of calcium binding proteins with multiple intracellular and extracellular roles. Expression of S100 was initially thought to be specific of cells derived from the neural crest, however, its presence has been confirmed in other cell types. While not exclusive to the neural crest, astrocytes and SCs are known to express high levels of S100B, thus expression of S100 was used to differentiate between SC and other cell types, such as fibroblasts, in primary cultures harvested from Sprague Dawley rats [74]. The estimated purity of the primary SC cultures harvested from sciatic nerves was 96%.

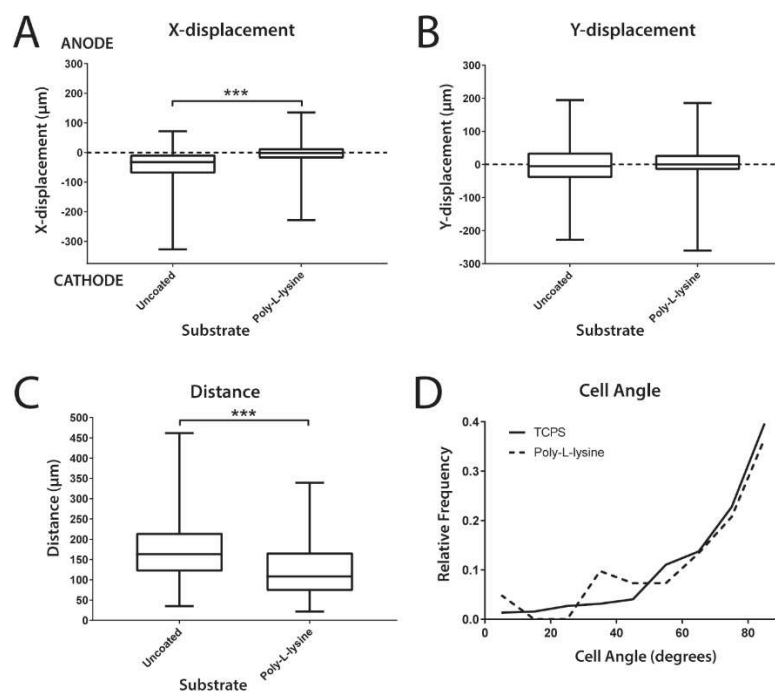


Figure 2.16 Schwann cell migration and alignment on poly-L-lysine (A-C) SCs showed reduced migratory response on PLL coated substrate, however (D) the alignment response was nearly equivalent.**

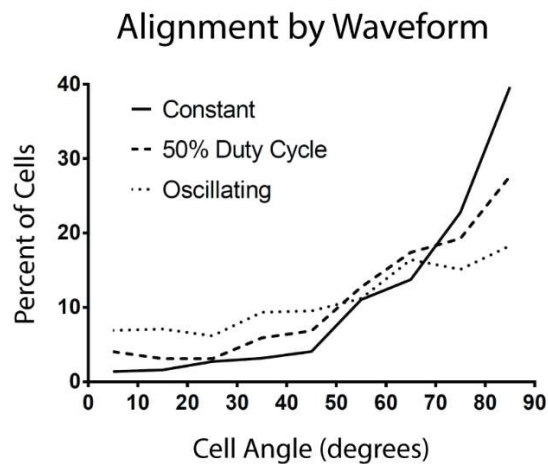


Figure 2.17 The effect of stimulation regime on Schwann cell alignment Plot showing SC alignment in 500 mV/mm EFs with varied stimulation waveform. This comparison revealed Con EF stimulation led to the greatest perpendicular cell alignment.

2.5 Variable Cell Density

The previous studies used a cell seeding density of 4,000 cells/cm² which limited the cell-cell interaction. A subsequent follow-up study was conducted to examine the effects of cell-cell interactions on the alignment response. Cell densities tested in this experiment ranged from 2,000 cells/cm² (where cells were mostly isolated) to 16,000 cells/cm² which was nearly confluent. Cell alignment varied by seeding density and was statistically significant in 200 and 500 mV/mm EFs ($p < 0.001$) but not for unstimulated trials ($p > 0.56$). The mean angle of alignment increased with cell density at 200 and 500 mV/mm Con EFs (Figure 2.18). Cells seeded at 16,000 cell/cm² in 500 mV/mm Con EFs had a mean cell angle of $69.5 \pm 20.2^\circ$ while cells seeded at 2,000 cells/cm² had a mean cell angle of $63.8 \pm 22.7^\circ$.

It is obvious single SCs are able to respond to electrical stimulation as demonstrated by the significant alignment in lowest seeding density compared to unstimulated controls which have a mean cell angle near 45° . The more confluent cultures may have higher alignment because of a reinforcing effect of aligned neighboring cells. Contact guided alignment has been shown in SCs with micropatterned substrates, but it can be reasonably assumed this would hold true for aligned neighboring cells [75].

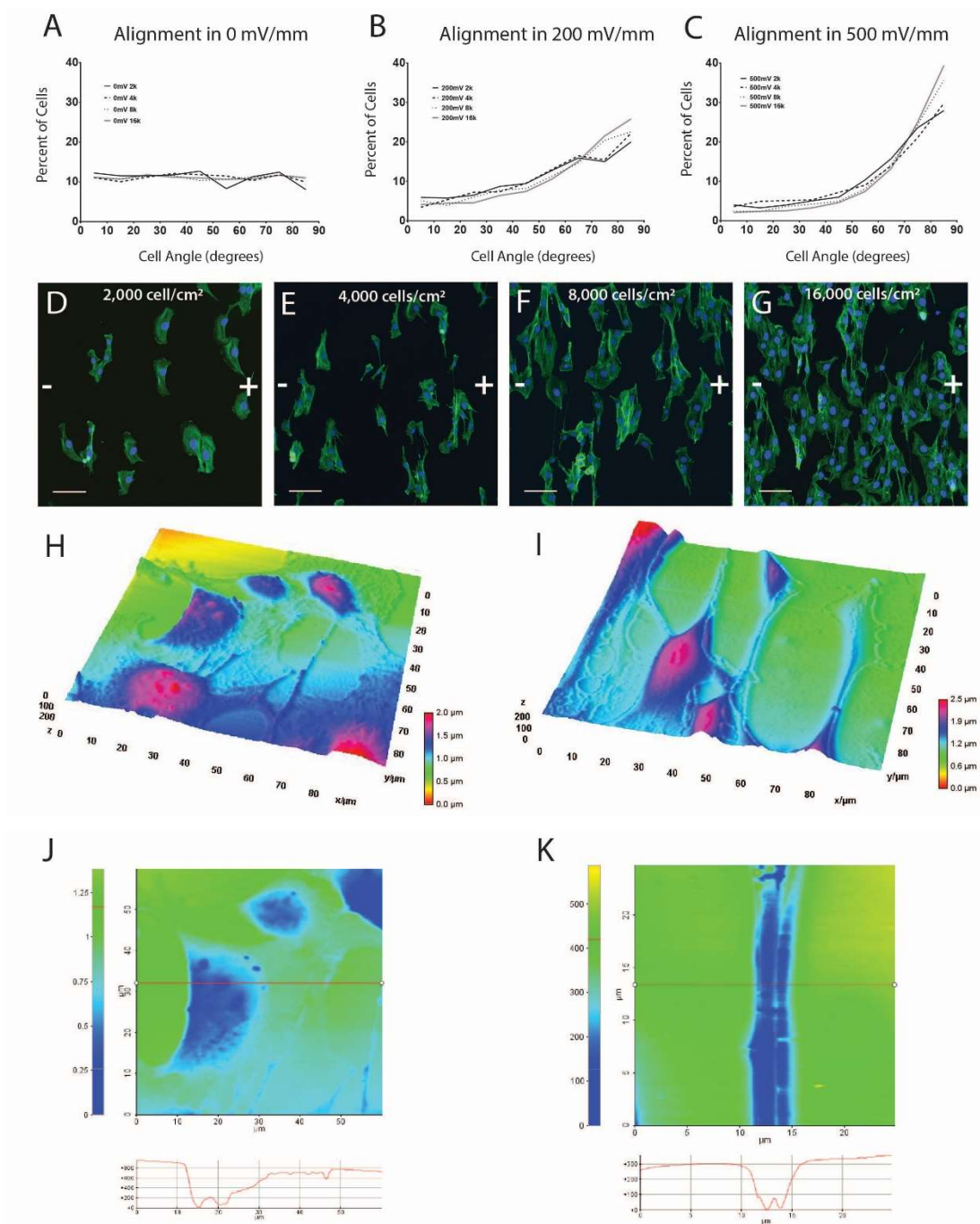


Figure 2.18 The effect of cell density on Schwann cell alignment

Cell density had no effect on alignment of (A) unstimulated SCs but correlated with increasing perpendicular cell alignment in (B) 200 and (C) 500 mV/mm Con EFs. (D -G) Representative images of variable seeding density in 500 mV/mm Con EFs. Actin shown in green. DAPI shown in blue. Scale bar 100 μm . Topographic AFM scans of SCs seeded at 16,000 cell/cm² (H) without EF stimulation and (I) with 500 mV/mm Con EF stimulation. (J) Cells were thickest near the nucleus ($\sim 1 \mu\text{m}$) while (K) SC extensions tended to be thinner ($\sim 300 \text{ nm}$).

3. SCHWANN CELL RESPONSE TO ELECTRIC FIELDS IN FIBRIN MATRICES

3.1 Introduction

Researchers have long known the use of conventional cell culture techniques (e.g. Petri dishes) carries undesired side-effects such as changes in morphology and gene expression. Pioneering experiments, utilizing the natural polymer collagen, have shown replication of tissue structures *in vitro* when cells are placed in a suitable 3D environment [76]. Understanding of the influence of cell-ECM signaling continues to grow, and in many cases three-dimensional cell culture (3DCC) provides a more relevant *in vitro* model for many systems. Previous studies investigating EF-stimulated SCs rely on conventional 2D cell culture techniques. Here the current investigation transitions to a 3D model of PNI, with hopes of obtaining more representative results of SC response electrical stimulation *in vivo*.

The preceding section, studying SC behavior in channel slides, provides a proof of concept, showing EFs influence SC migration, cell alignment, and morphology. Here we describe a more representative model of the injured nerve microenvironment using a fibrin hydrogel matrix. Fibrin is a major constituent of blood clots, and while it is not a part of healthy nerve ECM, it is found in nerve ECM after PNI (Figure 3.1) [77]. Inactive fibrinogen monomers are quickly polymerized into fibrin networks in the presence of the protease thrombin. Following neurotmesis, fibrin is upregulated throughout the nerve ECM and can provide a physical connection between nerve segments or between nerve and graft, depending on the surgical technique chosen. Fibroblasts migrate into the fibrin bridge, creating new ECM, and SC cross the lesion and form Bands of Bungner to guide neural growth cones extension into the distal endoneurial tubes. Nerve regeneration is only possible with a physical substrate for cells/axons to attach to, because fibrin makes up part of the injured nerve ECM, it is a logical choice for a matrix modeling PNI.

In order to generate EFs in 3D cell cultures, a custom channel slide was created which allowed for the separation of the slide and the cover. A PDMS coated cover glass was used to create a channel of uniform thickness. Once SCs were embedded in the fibrin matrix, the channel was completed with the addition of a polycarbonate cover piece.

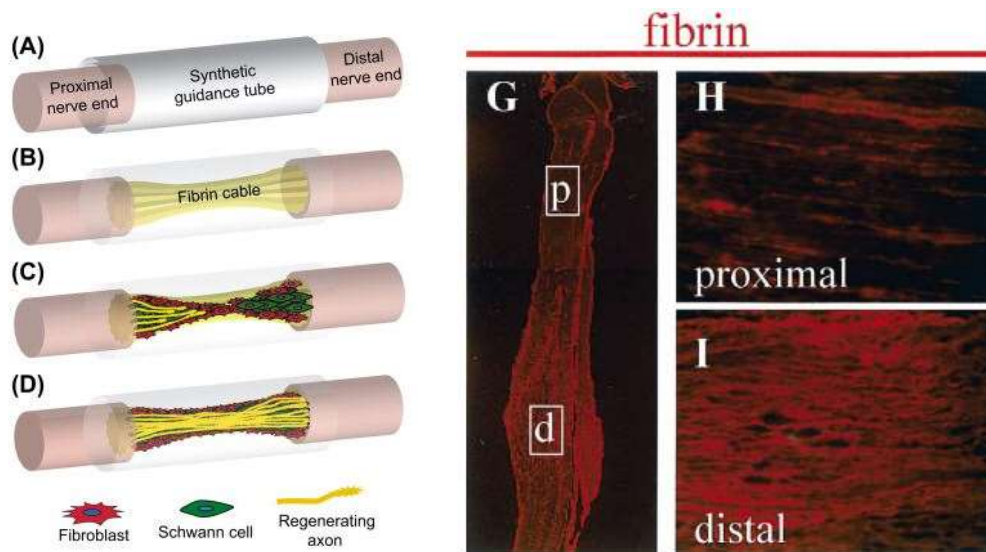


Figure 3.1 Fibrin is upregulated after nerve injury

(A-D) Fibrin can bridge gaps created by nerve injury. (G-I) Fibrin is primarily found distal to the site of injury. A-D Reprinted from *Biomaterials Science* (3rd edition), B. D. Ratner et al., © 2013 Elsevier. G-I Reprinted from *Neuroscience Letters*, K. Akassoglou et al., Fibrin is a regulator of Schwann cell migration after sciatic nerve injury in mice, 185-188, 338, © 2003, with permission from Elsevier.

3.2 Materials and Methods

3.2.1 PDMS Channel Slides

The IBIDI channel slides which proved very convenient for EF stimulation of 2D cultures could not be used for 3DCC EF experiments. Instead custom PDMS channel slides, which were compatible with 3DCC techniques, were used (Figure 3.2). Custom slides were created using 24 x 60-1.5 rectangular cover glass (Fisher Scientific) and Sylgard 184 silicone elastomer or polydimethylsiloxane (PDMS) (Dow). Cover glasses were arranged on a plastic sheet and covered with a thin layer (500 μm) of PDMS (12:1) and cured at room temperature. Once cured the PDMS was cut around the cover glass. A 40 x 4 mm channel was excised using a scalpel and circular wells were cut into the PDMS using a 6 mm biopsy punch. Once fabrication of the channel slides was complete, slides were sterilized with UV light.

EF stimulation of SCs in fibrin matrices required specialized cover pieces for the PDMS cover glass channel slides. A transparent cover was built using polycarbonate (McMaster Carr) and acrylic cement (Scigrip). Thick polycarbonate bars (12 mm) were cut and fixed to either end of a thin sheet (1.2 mm). Holes were drilled in the thick pieces creating reservoirs capable of holding volumes of 1 mL, these served as media stores for the cells. Polycarbonate cover pieces were extensively washed to remove cement residues and sterilized prior to use.

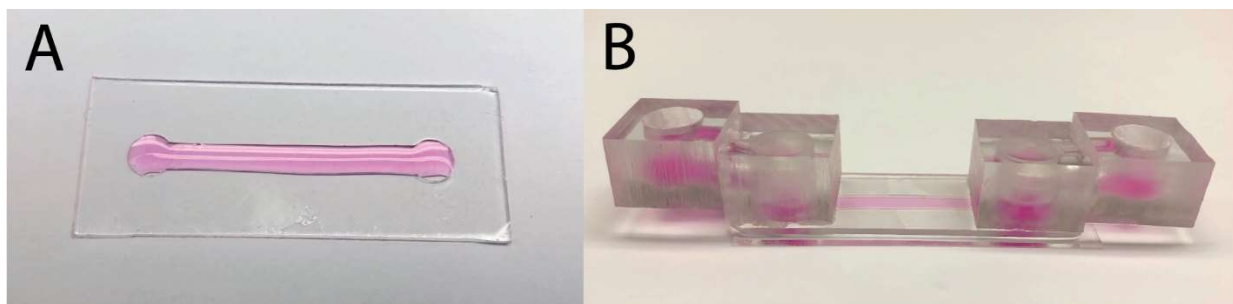


Figure 3.2 Custom PDMS channel slide

Custom PDMS channel slide is shown (A) without cover piece and (B) with cover piece.

3.2.2 Cell Culture

Cell culture techniques used in 3D fibrin matrix experiments were similar to those experiments completed using conventional 2D cell culture in IBIDI slides, described in section 2.2.1. The same RT4 rat SC line was utilized between passages 4–10, with identical procedures for passaging and media composition.

Embedding SCs in the fibrin matrices required seeding hours prior to EF stimulation, allowing the cells time to spread and extend processes. SCs were embedded uniformly in the fibrin matrix through the following process. Cells were detached from culture flasks using 0.25% trypsin then centrifuged and resuspended. The cell solution was diluted to 3×10^5 cells/mL. Next 20 μ L fibrinogen (Sigma Aldrich) solution (8 mg/mL in 0.9% NaCl) was combined with 16 μ L cell solution and the mixture was spread over the bottom of a PDMS channel slide. To initiate fibrinogen polymerization, 4 μ L thrombin (Sigma Aldrich) solution (20 units/mL in 200 mM CaCl₂) was then added to the channel and mixed briefly (4-5 seconds), before polymerization was evident, with a micropipette. Once all the components of the matrix were added, the slides were inverted and placed in the cell culture incubator for 30 minutes. After polymerization was complete, the matrix had a faint cloudy appearance. Some evaporation at the extremes of the channel was evident. The slides were turned right side up and penstrep media supplemented with 20 μ g/mL aprotinin (Sigma Aldrich) was added to the top of the fibrin gel. Cells were incubated 16-17 hours under standard cell culture conditions before initiating EF stimulation.

Prior to EF stimulation, the polycarbonate cover had to be attached to PDMS channel slides. Media was gently removed from the slides then sterile vacuum grease was applied to the PDMS around the channel and wells. The polycarbonate cover piece was lowered onto the slide and pressed gently, forming a watertight seal. Penstrep media supplemented with aprotinin was added to the reservoirs in the polycarbonate cover piece and flowed into the wells and channel of the channel slide.

The slides were moved into the temperature-controlled microscope chamber. Agar salt bridges, silver/silver chloride electrodes (120 mm length), vials filled with penstrep media, and a current generator were connected in a manner similar to that detailed in section 2.2.2 (Figure 2.1A), creating an electrolytic circuit. As with the 2D experiments, the duration of the EF stimulation was 6 hours. Once EF stimulation was finished the slides were moved into a laminar

flow hood and the cover piece was removed. Excess media and grease were wiped from the slide and cells were fixed with 4% PF solution.

3.2.3 Migration Tracking & Alignment

Throughout EF stimulation, phase contrast images of SCs in fibrin matrices were taken at five random locations every minute. Images were used for migration tracking using the same process described in section 2.2.3. Consistent with the setup used in 2D EF stimulation experiments, the EF vector was oriented horizontally, with the cathode (positive pole) located to the right and the anode to the left.

After fixation, the nucleus and actin cytoskeleton of cells were stained for imaging. Cells were permeabilized with 0.1% Triton X-100 for 30 minutes, then rinsed with PBS. Cell nuclei and actin cytoskeletons were stained overnight using a solution containing DAPI (300 nM) and phalloidin Alexa Fluor 488 (1:50). After removing the DAPI/phalloidin solution, slides were washed in PBS three times (5 min). SCs were imaged using the epi fluorescent microscope setup described in section 2.2.5. Higher resolution images of SC morphology were obtained using a Nikon A1R-MP confocal microscope, part of the Purdue Imaging Facility in the Bindley Bioscience Center.

3.2.4 Statistical Analysis

All trials were performed in triplicate ($n=3$). Non-parametric Kruskal-Wallis tests were used to compare path distance, X-displacement, Y-displacement and alignment data, as the samples were found to be heteroscedastic. Dunn's multiple comparisons test, a conservative post hoc test, was used to compare each EF condition to the control group. A significance level of $\alpha = 0.05$ was used.

3.3 Results

EF stimulation of SCs in fibrin matrices led to modest yet statistically significant changes in migration and cell alignment. Drastic changes in SC morphology were observed, however these changes existed in controls as well as EF-stimulated samples and can likely be attributed to the 3DCC method rather than being the result of EF stimulation.

3.3.1 Migration

EF stimulation of SCs within fibrin matrices led to modest anodal migration (Figure 3.3). Anodal SC galvanotaxis was most obvious in 500 mV/mm Con EFs and cells in this condition had a mean X-displacement of $33.7 \pm 27.8 \mu\text{m}$ ($5.6 \mu\text{m/hr}$). Cells in 200 mV/mm Con EFs and 200 & 500 mV/mm duty cycle EFs also had significant anodal migration compared to controls which had a mean X-displacement near the expected value of $0 \mu\text{m}$ ($4.4 \pm 33.9 \mu\text{m}$). As expected, no significant Y-displacement was observed for any EF stimulation conditions or controls. EF stimulation appeared to cause increased SC motility; cells in 200 & 500 mV/mm Con EFs as well as 200 mV/mm duty cycle EFs had significantly greater mean path distances (71.5 ± 28.4 , 75.0 ± 23.2 , and $76.5 \pm 27.9 \mu\text{m}$ respectively) than controls ($60.9 \pm 30.8 \mu\text{m}$).

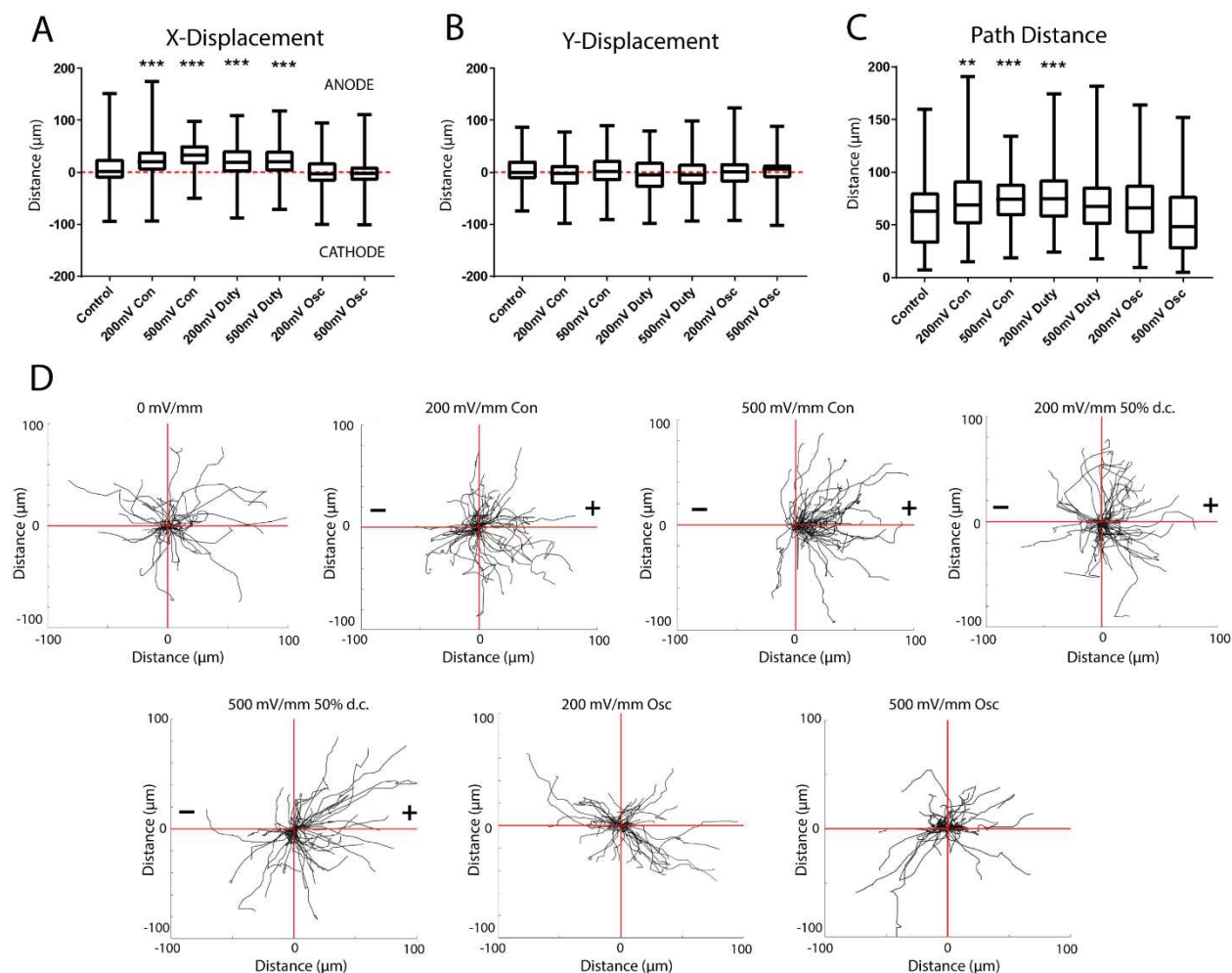


Figure 3.3 Schwann cell migration in fibrin matrices

SC (A) X-displacement, (B) Y-displacement, and (C) distance in fibrin matrices during 6-hour EF exposure. (D) Plots of migration path of 50 cells for each field strength tested.

3.3.2 Alignment

Upon application of EF stimulation, SCs cultured in fibrin hydrogels reoriented perpendicular to the field in 500 mV/mm Con EFs (Figure 3.4). The mean cell angle in this condition was significantly greater ($58.0 \pm 24.4^\circ$) than controls ($42.6 \pm 25.9^\circ$) ($p < 0.001$). Significantly different alignment was also detected in 200 mV/mm Osc EFs though the mean angle of cell alignment was only slightly greater ($48.2 \pm 27.4^\circ$) than controls ($p = 0.047$). All other EF stimulation conditions had cell angles which were not statistically different than controls.

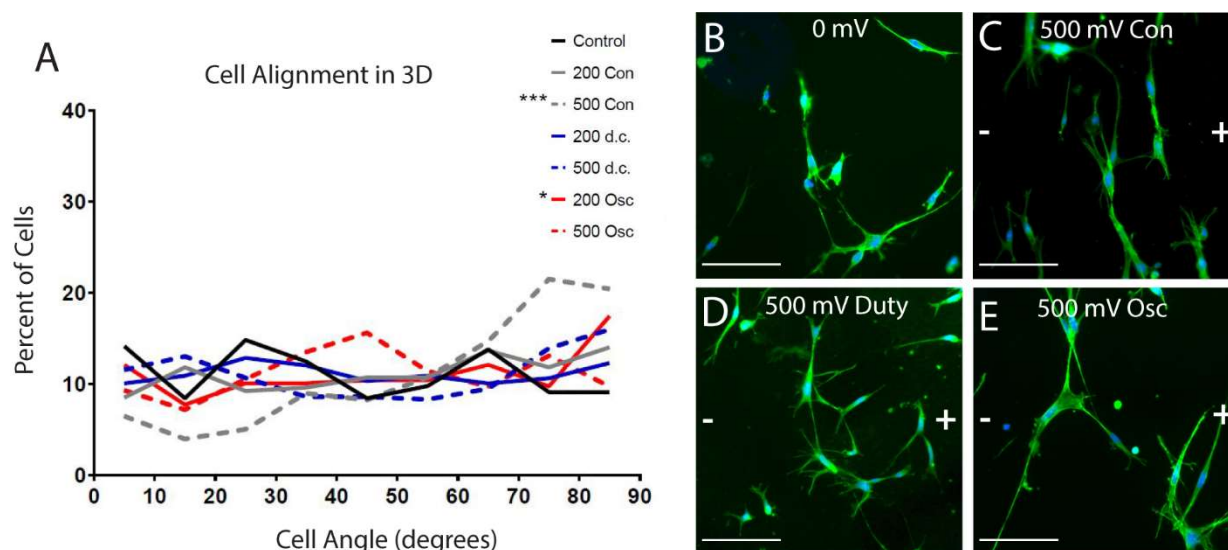


Figure 3.4 Electric field induced Schwann cell alignment in fibrin gels

(A) There was a slight bias toward perpendicular SC alignment in 500 mV/mm Con and 200 mV/mm Osc EFs. Images of SCs in fibrin matrices (B) without EF stimulation and with 500 mV/mm (C) Con EF, (D) 50% d.c. EF, and (E) Osc EF stimulation. Actin shown in green, DAPI in blue, and fibrin shown in red. Scale bar 100 μ m.

Table 2 Schwann cell alignment data in 3D fibrin matrices

Electric Field Condition (mV/mm)	Mean Angle (\pm std dev)	Percent $\geq 80^\circ$	
Control	0	$42.6 \pm 25.9^\circ$	9.1%
Constant EF	200	$48.3 \pm 25.8^\circ$	14.0%
	500	$58.0 \pm 24.4^\circ$	20.4%
50% Duty Cycle EF	200	$44.9 \pm 25.8^\circ$	12.2%
	500	$46.9 \pm 28.2^\circ$	16.0%
Oscillating EF	200	$48.3 \pm 27.5^\circ$	17.4%
	500	$46.7 \pm 24.6^\circ$	9.7%

3.4 Discussion

As a proof of concept, the previous chapter showed the sensitivity of SCs cultured in 2D to applied DC EFs, by quantifying changes in alignment, morphology, and migration. In this section we've begun a more thorough investigation into SC behavior by creating a more representative *in vitro* model of the nerve microenvironment after PNI using fibrin hydrogel. This experiment continues with the EF conditions from the 2D experiments in chapter 2 and highlights how cell-ECM interaction can alter cell response to applied EFs. The direction of galvanotaxis was reversed from the cathode in 2D to the anode in 3D matrices and SCs displayed diminished motility and alignment when cultured in 3D. Cell morphology was not quantified in 3D, however radical changes in cell shape were apparent between the 2D and 3D cell culture techniques. This study is the first to demonstrate SC migration and alignment in response to EF stimulation using 3DCC techniques. Moreover, when combined with findings from previous 2D SC EF testing, the results highlight the need to create an appropriate model for EF stimulation experiments in order for meaningful results to be obtained.

Electric stimulation of SCs in fibrin matrices induced very modest anodal migration in constant and duty cycle EFs, with the greatest rate of SC galvanotaxis ($5.6 \mu\text{m/hr}$) occurring in 500 mV/mm Con EFs. It is interesting to note the directional change in galvanotaxis between 2D (cathodal) and 3DCC (anodal) experiments. 3D SC galvanotaxis is an area of research previously unexplored, however, similar studies have been conducted using other cell types. Neural progenitor cells (NPCs) were found to migrate toward the cathode when exposed to applied EFs in an organotypic spinal cord slice as well as conventional 2D culture [78]. Three types of lung cancer cells were all found to have different migratory responses in gelatin matrices; CL1-0 cells showed no directional migration, while CL1-5 cells migrated cathodally and A549 cells displayed anodal migration [79]. While the direction of galvanotaxis varied by cell type, the migration direction of each cell type did not change when performed in planar 2D electrotactic experiments. Fibrin is reported to have an isoelectric point between 6.05-6.45, and would therefore have a net negative charge in the cell media used for EF experiments ($\text{pH} > 7.2$) [80]. The effect of substrate adhesion and charge have been identified as factors influencing cell response to EFs, and these could offer an explanation for the discrepancies in galvanotaxis between 2D and 3D cultures.

Reorientation of SCs perpendicular to the EF was observed to a much lesser extent in 3D fibrin matrices vs 2D culture. The mean cell alignment in 500 mV/mm Con EFs was $58.0 \pm 24.4^\circ$ in 3DCC compared to $68.1 \pm 19.0^\circ$ in 2D. It appears 500 mV/mm was the only EF stimulation condition that led to true perpendicular alignment. To our knowledge this is the first attempt to quantify cell alignment in 3D matrices after EF stimulation. The layer of fibrin in which SC were contained was so thin (around 30 μm) that this experiment might be more accurately considered quasi 2D culture. While SCs were dispersed in various z planes throughout the fibrin, individual cells were primarily planar ($\sim 5 \mu\text{m}$ thick) with the long axis of the cell lying nearly in the xy-plane. The thin fibrin layer and predominantly flat orientation of SCs facilitated the process for quantifying alignment in response to EF stimulation.

The final concentration of fibrin used (4 mg/mL) was chosen not only because of its mechanical properties (shear storage modulus of $30.4 \pm 18.1 \text{ Pa}$), but also because it is within the range of fibrinogen in human blood (1.6-4 mg/mL) [81]. The thickness of the fibrin matrices was not perfectly uniform, making tracking cell migration more challenging. Large fluctuations in the fibrin thickness were created during polymerization. Adhesion forces between the PDMS and liquid matrix ingredients created a concave meniscus within the channel, and the resulting matrix was much thicker near the channel edge ($\sim 100 \mu\text{m}$) than its center ($\sim 30 \mu\text{m}$). Minor inconsistencies in fibrin thickness (on the order of a few μm) may have been due to unequal polymerization rates (likely caused by imperfect mixing of the fibrinogen-cleaving protein thrombin). These undulations of the matrix and dispersion of cells in the z-direction resulted in only a portion of the cells within the field of view to be in focus. This problem was accentuated further by inevitable focus drift of the microscope over the course of the 6-hour experiments. Cells which remained within the field of view and reasonably in focus were used to quantify SC migration in fibrin matrices. Areas analyzed for migration and alignment were near the center of the channel where the matrix thickness was generally more uniform. For the reasons just described, the number of cells which could be tracked in each field of view was justifiably low.

The use of fibrin as the sole component of the matrix was one limitation of this particular nerve injury model. An ideal matrix would be an exact replica of nerve ECM after injury, containing fibrin as well as other native molecules including fibronectin and collagen [82]. Such an intricate matrix was not feasible for the current study, so to simplify the process only fibrin

was used. Fibrin is a legitimate choice to model the PNI microenvironment because it is not found in healthy peripheral nerve ECM, but is upregulated after injury [83].

SCs cultured in fibrin gel matrices displayed significantly altered morphologies compared to those observed in 2D culture; this comes as no surprise with the knowledge that SCs *in vivo* reside within a complex 3D environment. SCs cultured on IBIDI slides typically had one large lamellipodia and sometimes had 1-2 extensions, often at opposite ends of the cell. Characteristic of 2D cell culture, SCs were flat and non-dividing nuclei were usually large and somewhat circular (especially those not subject to EF stimulation). In 3DCC SCs took on a shape similar to a tree branch, and nuclei were often more oblong and appeared smaller when viewed in the xy-plane. Lamellipodia were much smaller if present at all in 3DCC, and cells displayed a more intricate branching morphology often with some long extensions and several shorter ones. Sometimes these cells had an overall bipolar morphology, but others took on a more complex branching shape. Some of the longest extensions observed exceeded 60 μm in length. The morphology of SCs is known to change drastically after nerve injury. Gomez-Sanchez et al. studied SC morphology in mice before and after nerve injury, they found that repair SCs were elongated (2-3 times longer than myelin or remak SCs) and branched [84]. By and large the descriptions and images provided by Gomez-Sanchez et al. more closely match the morphology of fibrin encapsulated SCs.

In this section we've established a model for PNI using physiologic concentration of fibrin and custom PDMS channel slides. Characterization of SC behavior in fibrin showed distinct responses to those observed in 2D. Generally, SCs were less motile and showed weaker reorientation to EFs, though significant perpendicular alignment was still observed. These studies provide a more representative model for SC response after PNI in the presence of an applied EF.

4. CONCLUSIONS AND FUTURE DIRECTIONS

4.1 Conclusions

The existing gold standards of neurorrhaphy and autologous grafting have been used for decades, with developed alternative strategies proving less effective. These current strategies accord that any physical gap created by injury should be bridged, thereby providing a connection for regenerating nerves. The actual regeneration is left entirely up to the native abilities of peripheral neurons and guiding SCs. We propose additional cues, in the form of applied electric fields, could modulate SC behavior by orienting cells in the direction of the nerve fiber or recruiting more cells to the lesion area and thereby improve recovery from PNI.

Mammalian cell responsiveness to EFs has been credibly demonstrated for decades. Modifications in cell behavior range from galvanotaxis and galvanotropism to altered gene expression and morphology. EFs have varying effects on different cell types, thus application of EFs to enhance peripheral nerve regrowth requires understanding of the influence of electrical stimulation on both neurons and SCs. Numerous studies have utilized peripheral neurons as test subjects and their responses to EFs are partially defined, however, the effects of electrical stimulation on the glia of the PNS are not well understood. In this study we have characterized SC behavior during EF stimulation, while simultaneously investigating parameters including field strength, stimulation waveform, cell density, substrate charge, and culture method.

In standard 2D culture, we defined changes in SC migration, alignment and morphology as a result of EF stimulation. Pronounced cell alignment perpendicular to the field was observed shortly after EF application and cathodal migration occurred at a rate of 7.5 $\mu\text{m/hr}$. Both findings are significant as they contradict previously published results. Alternate stimulation waveforms of 50% duty cycle and oscillating DC were tested, and while SCs displayed migratory and alignment responses, the magnitudes were reduced.

An overwhelming majority of cellular EF studies have been carried out using conventional 2D cell culture on plastic or coated glass slides. While these studies demonstrate the responsiveness of a number of cell types (including SCs), 3DCC studies provide a more accurate depiction of the effects of EFs *in vivo*. Thus, to more exactly characterize the response of SCs to DC EFs we created a fibrin-based model for nerve after PNI. The morphology of SCs

in this model more closely imitated reported *in vivo* descriptions of SCs after nerve injury. The cell alignment and migration responses observed in 2D channel slides were clearly different in 3D fibrin matrices. Bias toward perpendicular reorientation was substantially reduced while the rate of migration was diminished and the direction of galvanotaxis was reversed towards the anode. The presence of the fibrin can be considered a physical barrier which would explain the slowed migration and even the reorientation of the cells. Additionally, fibrin has been shown to inhibit SC migration compared to a fibronectin coated substrate [83]. The anodal galvanotaxis observed in 3DCC could be due to changes in adhesion compared to 2D. The three-dimensional fibrin allows for cell attachment throughout the cell surface, while 2D cultures restricted attachment to the adjacent surface. The discrepancies between the findings of the 2D and 3D studies highlight the need to conduct cellular EF stimulation studies in relevant 3D environments and also demonstrate some of the variables which can alter cell response to electrical stimulation. Potential applications of EFs *in vivo* should be careful to consider all variables.

4.2 Future Directions

Current treatments for PNIs provide a physical connection between severed nerves but lack additional regenerative cues at the cellular level. Electrical stimulation is one potential method for providing a biophysical signal to cells within a regenerating nerve. Future investigations into EF-mediated SC behaviors might consider variables such as stimulation duration and ECM compositions in 3DCC. Ultimately, demonstration of DC EF-induced regeneration in animal models would be necessary before electrical stimulation of damaged nerve can be translated to humans.

The amount of byproduct created by EFs is directly related to field strength, hence utilizing weaker EFs would reduce byproduct complications. Long term cellular studies (days to weeks) might reveal a lower EF threshold for inducing alignment or migratory responses in SCs. Application of EFs for multiple days could also expose delayed effects of electrical stimulation on SCs not apparent after 6-hour experiments.

The fibrin matrix is a simple yet rational model for lesioned peripheral nerve and adjacent tissue, however, SCs are known to migrate from distal areas of the damaged nerve which may not have a large concentration of fibrin. The initial microenvironment of these cells may be different from the lesion and more similar to the ECM of undamaged peripheral nerve.

Additional EF studies using matrices more similar to undamaged peripheral nerve would be a more appropriate study for these cells and might suggest differential migration patterns depending on ECM composition.

With additional knowledge from extended EF stimulation and varied matrix trials, an optimal application for DC EFs for PNI could be designed. Collectively our results suggest the alignment response is more robust than galvanotaxis in SCs, so greatest benefit for promoting axon regeneration may result from aligned SCs. The perpendicular reorientation of SC would require the EF to run orthogonal to the nerve fiber in order to produce the desired alignment. Any directed migration under this setup would draw SCs laterally toward one side of the nerve, which would not be conducive for axon regeneration. The response of neurons themselves should obviously be of primary concern when considering the EF orientation. Sympathetic neurons and dorsal root ganglion have shown a related perpendicular orientation to EFs with neurites extending orthogonally to the EF vector [58]. In theory, the electrode placement just described would not only promote SC alignment along the nerve fiber, but also neurite extension. An animal model could be used to test the overall regenerative impact of DC EFs on neurons and SCs in peripheral nerve. The femoral nerve of rats would be one suitable option for DC EF stimulation as it has been used previously with success using low frequency AC stimulation [85]. Results from animal testing would provide a realistic indication of the worth of DC electrical stimulation to treat PNIs in humans.

APPENDIX

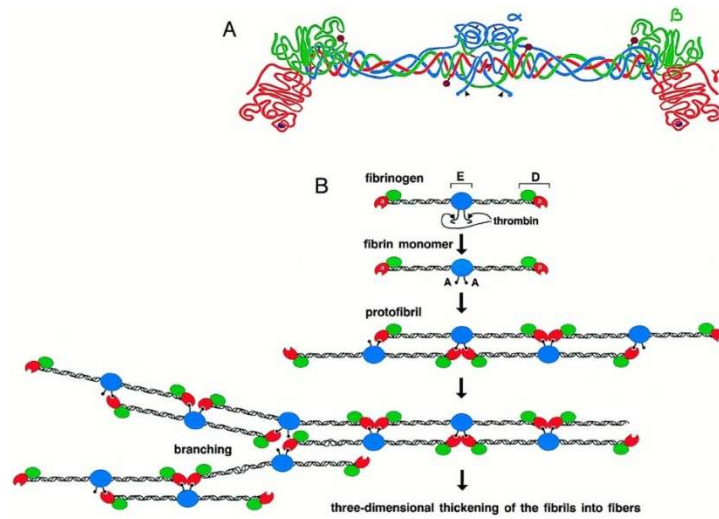


Figure 4.1 Fibrinogen/fibrin structure

Fibrinogen is polymerized into fibrin upon addition of the protease thrombin.

REFERENCES

- [1] K. Brattain, “Analysis of the Peripheral Nerve Repair Market in the United States,” Minneapolis, MN, 2009.
- [2] H. J. Seddon, “Three Types of Nerve Injuries,” *Brain*, vol. 66, pp. 238–283, 1943.
- [3] S. Sunderland, “Degeneration. Regeneration. A Classification of Nerve Injury,” in *Nerves and Nerve Injuries*, Edinburgh and London: E.& S. Livingstone LTD, 1968, pp. 68–127.
- [4] T. M. Brushart, “Clinical Nerve Repair And Grafting,” in *Nerve Repair*, New York, NY: Oxford University Press, 2011, pp. 104–134.
- [5] S. Sunderland, “The Anatomy and Physiology of Nerve Injury,” *Muscle and Nerve*, vol. 13, pp. 771–784, 1990.
- [6] D. Grinsell and C. P. Keating, “Peripheral Nerve Reconstruction after Injury: A Review of Clinical and Experimental Therapies,” *Biomed Res. Int.*, vol. 2014, pp. 1–13, 2014.
- [7] A. Narakas, “The Use of Fibrin Glue in Repair of Peripheral Nerves,” *Orthop. Clin. North Am.*, vol. 19, no. 1, pp. 187–199, 1988.
- [8] R. Tse and J. H. Ko, “Nerve Glue for Upper Extremity Reconstruction,” *Hand Clin.*, vol. 28, no. 4, pp. 529–540, 2012.
- [9] C. L. F. Temple, D. C. Ross, C. E. Dunning, and J. A. Johnson, “Resistance to Disruption and gapping of peripheral nerve repairs: an in vitro biomechanical assessment of techniques,” *J. Reconstr. Microsurg.*, vol. 20, no. 8, pp. 645–650, 2004.
- [10] N. I. Cruz, N. Debs, and R. E. Fiol, “Evaluation of fibrin glue in rat sciatic nerve repairs,” *Plastic and Reconstructive Surgery*, vol. 78, no. 3, pp. 369–373, 1986.
- [11] A. M. Moore, W. Z. Ray, K. E. Chenard, T. Tung, and S. E. Mackinnon, “Nerve allotransplantation as it pertains to composite tissue transplantation,” *Hand*, vol. 4, no. 3, pp. 239–244, 2009.
- [12] E. L. Whitlock *et al.*, “Processed allografts and type I collagen conduits for repair of peripheral nerve gaps,” *Muscle and Nerve*, vol. 39, no. 6, pp. 787–799, 2009.
- [13] W. Chang, M. B. Shah, P. Lee, and X. Yu, “Tissue-engineered spiral nerve guidance conduit for peripheral nerve regeneration,” *Acta Biomater.*, vol. 73, pp. 302–311, 2018.
- [14] C. M. Owens, F. Marga, G. Forgacs, and C. M. Heesch, “Biofabrication and testing of a fully cellular nerve graft,” *Biofabrication*, vol. 5, no. 4, 2013.

- [15] A. M. Moore *et al.*, “Controlled Delivery of Glial Cell Line–Derived Neurotrophic Factor Enhances Motor Nerve Regeneration,” *J. Hand Surg. Am.*, vol. 35, no. 12, pp. 2008–2017, 2010.
- [16] D. Weber, RA. Bredenbach, WE. Brown, RE. Jabaley, ME. Mass, “A randomized prospective study of polyglycolic acid conduits for digital nerve reconstruction in humans,” *Plast. Reconstr. Surg.*, vol. 106, no. 5, pp. 1036–1045, 2000.
- [17] A. C. J. Ruijs, J. B. Jaquet, S. Kalmijn, H. Giele, and S. E. R. Hovius, “Median and ulnar nerve injuries: A meta-analysis of predictors of motor and sensory recovery after modern microsurgical nerve repair,” *Plast. Reconstr. Surg.*, vol. 116, no. 2, pp. 484–494, 2005.
- [18] K. R. Jessen and R. Mirsky, “The repair Schwann cell and its function in regenerating nerves,” *J. Physiol.*, vol. 594, no. 13, pp. 3521–3531, 2016.
- [19] R. P. Bunge, “The role of the Schwann cell in trophic support and regeneration,” *J. Neurol.*, vol. 242, pp. S19–S21, 1994.
- [20] S. M. Hall, “Regeneration in Cellular and Acellular Autografts in the Peripheral Nervous System,” *Neuropathol. Appl. Neurobiol.*, vol. 12, no. 1, pp. 27–46, 1986.
- [21] Y. Y. Chen, D. McDonald, C. Cheng, D. W. Zochodne, B. Magnowski, and J. Durand, “Axon and Schwann Cell Partnership During Nerve Regrowth,” *J. Neuropathol. Exp. Neurol.*, vol. 64, no. 7, pp. 613–622, 2005.
- [22] K. Torigoe, H.-F. Tanaka, A. Takahashi, A. Awaya, and K. Hashimoto, “Basic Behavior of Migratory Schwann Cells in Peripheral Nerve Regeneration,” *Exp. Neurol.*, vol. 137, no. 2, pp. 301–308, 1996.
- [23] R. Shi and R. Borgens, “Three-Dimensional Gradients of Voltage During Development of the Nervous System as Invisible Coordinates for the Establishment of Embryonic Pattern,” *Dev. Dyn.*, vol. 202, pp. 101–114, 1995.
- [24] K. B. Hotary and K. R. Robinson, “Endogenous electrical currents and the resultant voltage gradients in the chick embryo,” *Dev. Biol.*, vol. 140, no. 1, pp. 149–160, 1990.
- [25] R. H. W. Funk, “Endogenous electric fields as guiding cue for cell migration,” *Front. Physiol.*, vol. 6, no. 143, pp. 1–8, 2015.
- [26] L. F. Jaffe, “The role of ionic currents in establishing developmental pattern,” *Philos. Trans. R. Soc. Lond. B. Biol. Sci.*, vol. 295, pp. 553–566, 1981.
- [27] M. E. M. Metcalf and R. B. Borgens, “Weak applied voltages interfere with amphibian morphogenesis and pattern,” *J. Exp. Zool.*, vol. 268, no. 4, pp. 323–338, 1994.
- [28] K. B. Hotary and K. R. Robinson, “Endogenous electrical currents and voltage gradients in *Xenopus* embryos and the consequences of their disruption,” *Dev. Biol.*, vol. 166, pp. 789–800, 1994.

- [29] M. E. McGinnis and J. W. Vanable, "Electrical Fields in *Notophthalmus viridescens* Limb Stumps," *Dev. Biol.*, vol. 116, pp. 184–193, 1986.
- [30] R. F. Stump and K. R. Robinson, "Ionic current in *Xenopus* embryos during neurulation and wound healing," in *Ionic Currents in Development*, R. Nuccitelli, Ed. New York, NY: Alan R. Liss Inc, 1986, pp. 223–230.
- [31] L. R. Robinson, "The effects of electric fields on wound healing in *Notophthalmus viridescens*," Purdue University, 1985.
- [32] A. T. Barker, L. F. Jaffe, and J. W. Vanable, "The glabrous epidermis of cavies contains a powerful battery," *Am. J. Physiol. Integr. Comp. Physiol.*, vol. 242, no. 3, pp. R358–R366, 2017.
- [33] B. Reid, B. Song, C. D. McCaig, and M. Zhao, "Wound healing in rat cornea: the role of electric currents," *FASEB J.*, vol. 19, no. 3, pp. 379–386, 2005.
- [34] B. Reid, E. O. Graue-Hernandez, M. J. Mannis, and M. Zhao, "Modulating endogenous electric currents in human corneal wounds—a novel approach of bioelectric stimulation without electrodes," *Cornea*, vol. 30, no. 3, pp. 338–343, 2011.
- [35] R. Shi and R. B. Borgens, "Embryonic Neuroepithelial Sodium Transport, the Resulting Physiological Potential, and Cranial Development," *Dev. Biol.*, vol. 165, pp. 105–116, 1994.
- [36] A. M. Rajnicek, R. F. Stump, and K. R. Robinson, "An Endogenous Sodium Current May Mediate Wound Healing in *Xenopus* Neurulae," *Dev. Biol.*, vol. 128, no. 2, pp. 290–299, 1988.
- [37] H.-F. Chang, Y.-S. Lee, T. K. Tang, and J.-Y. Cheng, "Pulsed DC Electric Field–Induced Differentiation of Cortical Neural Precursor Cells," *PLoS One*, vol. 11, no. 6, pp. 1–16, 2016.
- [38] A. Cossarizza *et al.*, "Extremely low frequency pulsed electromagnetic fields increase cell proliferation in lymphocytes from young and aged subjects," *Biochem. Biophys. Res. Commun.*, vol. 160, no. 2, pp. 692–698, 1989.
- [39] P. G. Chao, H. H. Lu, C. T. Hung, S. B. Nicoll, and J. C. Bulinski, "Effects of Applied DC Electric Field on Ligament Fibroblast Migration and Wound Healing," *Connect. Tissue Res.*, vol. 48, no. 4, pp. 188–197, 2007.
- [40] N. Patel and M.-M. Poo, "Orientation of neurite growth by extracellular electrical fields," *J. Neurosci.*, vol. 2, no. 4, pp. 483–496, 1982.
- [41] A. N. Koppes *et al.*, "Electrical Stimulation of Schwann Cells Promotes Sustained Increases in Neurite Outgrowth," *Tissue Eng. Part A*, vol. 20, no. 3, pp. 494–506, 2013.

- [42] R. B. Borgens, R. Shi, T. J. Mohr, and C. B. Jaeger, "Mammalian Cortical Astrocytes Align Themselves in a Physiological Voltage Gradient," *Exp. Neurol.*, vol. 128, pp. 41–49, 1994.
- [43] C. E. Pullar and R. R. Isseroff, "Cyclic AMP mediates keratinocyte directional migration in an electric field," *J. Cell Sci.*, vol. 118, no. 9, pp. 2023–2034, 2005.
- [44] L. Li *et al.*, "Electric fields guide migration of epidermal stem cells and promote skin wound healing," *Wound Repair Regen.*, vol. 20, no. 6, pp. 840–851, 2012.
- [45] A. Guo *et al.*, "Effects of Physiological Electric Fields on Migration of Human Dermal Fibroblasts," *J. Invest. Dermatol.*, vol. 130, no. 9, pp. 2320–2327, 2010.
- [46] V. A. McBain, J. V. Forrester, and C. D. McCaig, "HGF, MAPK, and a small physiological electric field interact during corneal epithelial cell migration," *Investig. Ophthalmol. Vis. Sci.*, vol. 44, no. 2, pp. 540–547, 2003.
- [47] L. F. Jaffe and M. -M Poo, "Neurites grow faster towards the cathode than the anode in a steady field," *J. Exp. Zool.*, vol. 209, no. 1, pp. 115–127, 1979.
- [48] L. Pan and R. Ben Borgens, "Perpendicular organization of sympathetic neurons within a required physiological voltage," *Exp. Neurol.*, vol. 222, no. 1, pp. 161–164, 2010.
- [49] J. K. Alexander, B. Fuss, and R. J. Colello, "Electric field-induced astrocyte alignment directs neurite outgrowth," *Neuron Glia Biol.*, vol. 2, no. 2, pp. 93–103, 2006.
- [50] B. Zhu *et al.*, "Electric signals regulate the directional migration of oligodendrocyte progenitor cells (OPCs) via $\beta 1$ integrin," *Int. J. Mol. Sci.*, vol. 17, no. 11, 2016.
- [51] R. Nuccitelli and C. A. Erickson, "Embryonic Cell Motility Can Be Guided by Physiological Electric Fields," *Exp. Cell Res.*, vol. 147, no. 1, pp. 195–201, 1983.
- [52] A. M. Rajnicek, K. R. Robinson, and C. D. McCaig, "The Direction of Neurite Growth in a Weak DC Electric Field Depends on the Substratum: Contributions of Adhesivity and Net Surface Charge," *Dev. Biol.*, vol. 203, pp. 412–423, 1998.
- [53] S. Shapiro *et al.*, "Oscillating field stimulation for complete spinal cord injury in humans: a Phase 1 trial," *J. Neurosurg. Spine*, vol. 2, no. 1, pp. 3–10, 2005.
- [54] R. B. Borgens *et al.*, "An Imposed Oscillating Electrical Field Improves the Recovery of Function in Neurologically Complete Paraplegic Dogs," *J. Neurotrauma*, vol. 16, no. 7, pp. 639–657, 1999.
- [55] C. D. McCaig, "Spinal neurite reabsorption and regrowth in vitro depend on the polarity of an applied electric field," *Development*, vol. 100, no. 1, pp. 31–41, 1987.

- [56] R. B. Borgens, A. R. Blight, and M. E. McGinnis, "Behavioral Recovery Induced by Applied Electric Fields after Spinal Cord Hemisection in Guinea Pig," *Am. Assoc. Adv. Sci.*, vol. 238, no. 4825, pp. 366–369, 1987.
- [57] R. B. Borgens, A. R. Blight, and M. E. McGinnis, "Functional recovery after spinal cord hemisection in guinea pigs: The effects of applied electric fields," *J. Comp. Neurol.*, vol. 296, no. 4, pp. 634–653, 1990.
- [58] L. Pan and R. Ben Borgens, "Strict Perpendicular Orientation of Neural Crest-Derived Neurons In Vitro Is dependent on an Extracellular Gradient of Voltage," *J. Neurosci. Res.*, vol. 90, no. 7, pp. 1335–1346, 2012.
- [59] J. Song *et al.*, "Polymerizing Pyrrole Coated Poly (l-lactic acid-co- ϵ -caprolactone) (PLCL) Conductive Nanofibrous Conduit Combined with Electric Stimulation for Long-Range Peripheral Nerve Regeneration," *Front. Mol. Neurosci.*, vol. 9, pp. 1–13, 2016.
- [60] A. N. Koppes, A. M. Seggio, and D. M. Thompson, "Neurite outgrowth is significantly increased by the simultaneous presentation of Schwann cells and moderate exogenous electric fields," *J. Neural Eng.*, vol. 8, no. 4, pp. 1–13, 2011.
- [61] H. T. Nguyen, C. Wei, J. K. Chow, L. Nguy, H. K. Nguyen, and C. E. Schmidt, "Electric field stimulation through a substrate influences Schwann cell and extracellular matrix structure," *J. Neural Eng.*, vol. 10, no. 4, pp. 1–12, 2013.
- [62] L. Yao, Y. Li, J. Knapp, and P. Smith, "Exploration of Molecular Pathways Mediating Electric Field-Directed Schwann Cell Migration by RNA-seq," *J. Cell. Physiol.*, vol. 230, no. 7, pp. 1515–1524, 2015.
- [63] M. J. McKasson, L. Huang, and K. R. Robinson, "Chick embryonic Schwann cells migrate anodally in small electrical fields," *Exp. Neurol.*, vol. 211, no. 2, pp. 585–587, 2008.
- [64] S. M. Hall, "The Effect of Inhibiting Schwann Cell Mitosis on the Re-Innervation of Acellular Autografts in the Peripheral Nervous System of the Mouse," *Neuropathol. Appl. Neurobiol.*, vol. 12, no. 4, pp. 401–414, 1986.
- [65] Y. Wei *et al.*, "An improved method for isolating Schwann cells from postnatal rat sciatic nerves," *Cell Tissue Res.*, vol. 337, no. 3, pp. 361–369, 2009.
- [66] A. Seluanov, A. Vaidya, and V. Gorbunova, "Establishing Primary Adult Fibroblast Cultures From Rodents," *J. Vis. Exp.*, vol. 44, pp. 1–4, 2010.
- [67] K. Talat, S. Sayers, and N. Chauhan, "Effect of Applied Electric Field on Atrocytic Scar Formation After Spinal Cord Injury," in *Electricity and Magnetism in Biology and Medicine*, F. Bersani, Ed. Boston, MA: Springer, 1999, pp. 887–890.
- [68] R. B. Borgens, "Electrically mediated regeneration and guidance of adult mammalian spinal axons into polymeric channels," *Neuroscience*, vol. 91, no. 1, pp. 251–264, 1999.

- [69] E. K. Onuma, "Electric field-directed cell shape changes, displacement, and cytoskeletal reorganization are calcium dependent," *J. Cell Biol.*, vol. 106, no. 6, pp. 2067–2075, 1988.
- [70] L. F. Jaffe, "Electrophoresis along cell membranes," *Nature*, vol. 265, pp. 600–602, 1977.
- [71] M. M. Poo and K. R. Robinson, "Electrophoresis of concanavalin A receptors along embryonic muscle cell membrane," *Nature*, vol. 265, no. 5595, pp. 602–605, 1977.
- [72] D. Bonazzi and N. Minc, "Dissecting the Molecular Mechanisms of Electrotactic Effects," *Adv. Wound Care*, vol. 3, no. 2, pp. 139–148, 2014.
- [73] J. Han, X.-L. Yan, Q.-H. Han, Y.-J. Li, Z.-J. Du, and Y.-N. Hui, "Integrin β 1 subunit signaling is involved in the directed migration of human retinal pigment epithelial cells following electric field stimulation," *Ophthalmic Res.*, vol. 45, no. 1, pp. 15–22, 2011.
- [74] P. H. Kuberappa, B. S. Bagalad, A. Ananthaneni, M. A. Kiresur, and G. V. Srinivas, "Certainty of S100 from physiology to pathology," *J. Clin. Diagnostic Res.*, vol. 10, no. 6, pp. 10–15, 2016.
- [75] B. W. Tuft *et al.*, "Photopolymerized microfeatures for directed spiral ganglion neurite and Schwann cell growth," *Biomaterials*, vol. 34, no. 1, pp. 42–54, 2013.
- [76] M. J. Bissell, "The Differentiated State of Normal and Malignant Cells or How to Define a 'Normal' Cell in Culture," *Int. Rev. Cytol.*, vol. 70, no. C, pp. 27–100, 1981.
- [77] K. Akassoglou, W. M. Yu, P. Akpinar, and S. Strickland, "Fibrin inhibits peripheral nerve remyelination by regulating Schwann cell differentiation," *Neuron*, vol. 33, no. 6, pp. 861–875, 2002.
- [78] X. Meng *et al.*, "Electric Field-controlled Directed Migration of Neural Progenitor Cells in 2D and 3D Environments," *J. Vis. Exp.*, no. 60, pp. 4–7, 2012.
- [79] Y. S. Sun, S. W. Peng, K. H. Lin, and J. Y. Cheng, "Electrotaxis of lung cancer cells in ordered three-dimensional scaffolds," *Biomicrofluidics*, vol. 6, no. 1, pp. 1–14, 2012.
- [80] H. Arnesen, "Characterization of Fibrinogen and Fibrin Degradation Products by Isoelectric Focusing in Polyacrylamide Gel," *Thromb. Res.*, vol. 4, pp. 861–868, 1974.
- [81] R. Asselta, S. Duga, and M. L. Tenchini, "The molecular basis of quantitative fibrinogen disorders," *J. Thromb. Haemost.*, vol. 4, no. 10, pp. 2115–2129, 2006.
- [82] A. Baron-Van Evercooren, A. Gansmuller, M. Gumpel, N. Baumann, and H. K. Kleinman, "Schwann Cell Differentiation in vitro: Extracellular Matrix Deposition and Interaction," *Dev. Neurosci.*, vol. 8, no. 3, pp. 182–196, 1986.
- [83] K. Akassoglou, P. Akpinar, S. Murray, and S. Strickland, "Fibrin is a regulator of Schwann cell migration after sciatic nerve injury in mice," *Neurosci. Lett.*, vol. 338, no. 3, pp. 185–188, 2003.

- [84] J. A. Gomez-Sanchez *et al.*, “After nerve injury, lineage tracing shows that myelin and Remak Schwann cells elongate extensively and branch to form repair Schwann cells, which shorten radically on re-myelination.,” *J. Neurosci.*, vol. 37, no. 37, pp. 9086–9099, 2017.
- [85] N. M. Geremia, T. Gordon, T. M. Brushart, A. A. Al-Majed, and V. M. K. Verge, “Electrical stimulation promotes sensory neuron regeneration and growth-associated gene expression,” *Exp. Neurol.*, vol. 205, no. 2, pp. 347–359, 2007.

PUBLICATIONS

S. J. Bunn, A. Lai, and J. Li, “DC Electric Fields Induce Perpendicular Alignment and Enhanced Migration in Schwann Cell Cultures,” *Ann. Biomed. Eng.*, vol. 47, no. 7, pp. 1584–1595, 2019.

B. J. Green *et al.*, “Effect of Molecular Weight and Functionality on Acrylated Poly(caprolactone) for Stereolithography and Biomedical Applications,” *Biomacromolecules*, vol. 19, no. 9, pp. 3682–3692, 2018.